Temperature and Salinity Variability in Thermohaline Staircase Layers

by

David Allen Stuebe

B.S. Earth Ocean Science
Duke University, Trinity College of Arts and Sciences, 2002

Submitted in partial fulfillment of the requirements for the degree of

Master of Science

at the

MASSACHUSETTS INSTITUTE OF TECHNOLOGY

and the

WOODS HOLE OCEANOGRAPHIC INSTITUTION

September 2005

© David Allen Stuebe, MMV. All rights reserved.

The author hereby grants to MIT and WHOI permission to reproduce and distribute publicly paper and electronic copies of this thesis document in whole or in part.

Author . . . .
Department of Physical Oceanography
Defense Date: May 25, 2005
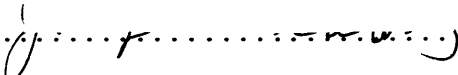
Certified by . . . .
Raymond Schmitt
Senior Scientist
Thesis Supervisor

Accepted by . . . .
Joseph Pedlosky
Joint Committee on Physical Oceanogrpahy Chairman
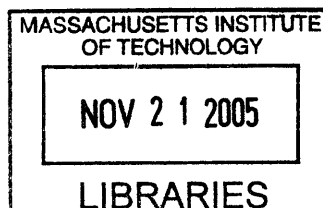
Temperature and Salinity Variability in Thermohaline Staircase Layers

by

David Allen Stuebe

Submitted to the Massachusetts Institute of Technology
and the Woods Hole Oceanographic Institution
in partial fulfillment of the requirements for the degree of
Master of Science

Abstract

A moored profiler record from the western tropical North Atlantic provides the first continuous time series of temperature, salinity and velocity profiles in a thermohaline staircase. Variations in the intensity of layering and the evolution of layer properties are well documented during the 4.3 month record. Such staircases are the result of strong salt fingering at the interfaces between the mixed layers, and these data provide unique insights into the dynamics of salt fingers. In particular, a striking linear correlation between the temperature and salinity of the layers may be interpreted as resulting from vertical salt finger flux divergences. Data from this record allow new interpretations of previous work on this topic by McDougall (1991).

Thesis Supervisor: Raymond Schmitt
Title: Senior Scientist

Acknowledgments

Science is presented to the public as glamorous and as tedious in roughly equal proportions. Neither aspect is presented accurately though the dichotomy is certainly real. For all the many people who have shared in and returned my excitement for science, thank you for your support in this wonderful, creative endeavor. It is the to-often unspoken part of the scientific method, the formation of scientific ideas about the world which should be celebrated as glamorous, but more importantly, as collaborative. My friends, family and colleagues have also played an equally important role in the rigorous, and often tedious, aspects of science as well. Thank you all for your uncountable hours of help and support in every aspect from correcting typo's to constructing models.

My advisor, Ray Schmitt deserves special thanks for supporting me in my work since I started as a summer fellow at WHOI four years ago.

Contents

List of Figures

List of Tables

Chapter 1

Introduction

Salt fingers are more than an elegant curiosity of fluid physics in oceanography. There is mounting evidence that the difference between vertical transport of heat and of salt which results from salt fingering plays an significant role in oceanic mixing. Salt fingers impact a range of scales from frontal intrusions to regional water mass conversion through diabatic flux and in this capacity may even influence the thermohaline circulation (Zhang and Schmitt, 2000).

In a recent study, the Salt Finger Tracer Release Experiment (SFTRE) sought to measure the fluxes due to salt fingering through the extensive thermohaline staircase observed in the Western Tropical Atlantic (Schmitt et al, 2005). A combination of techniques was employed, including direct microstructure measurements from the High Resolution Profiler (HRP) and a tracer release of Sulfur Hexaflouride (SF_6), to allow comparison of independent estimates of the vertical eddy diffusivity of salt.

Spatial surveys during the Caribbean Sheets and Layers Transects (C-SALT, 1985) mapped the layers of the thermohaline staircase which occupy the thermocline of the water column east of Barbados. In this region Subtropical Underwater and Upper Antarctic Intermediate Water converge, one on top of the other (Schmitt et al., 1987). The superposition of these water-masses creates one of the strongest density compensated stratifications of temperature and salinity in the ocean: the salinity decreases by more than two practical salinity units (~ 37.3 to ~ 35) between 100 and 700 meters depth. Furthermore, there is evidence that physical processes in the region result in a large diabatic salt flux between these two water masses as they transit to the Florida Straight (Schmitz et al., 1993).

The C-SALT observations not only provide motivation to quantify the total flux of salt, but also to examine the flux convergence which maintains the linear relationship of temperature and salinity in the layers observed by Schmitt et al. (1987). They show that the potential temperature and salinity in a layer are linearly related over the 400 km^2 of the C-SALT survey by selecting temperature and salinity values from the layers observed in each of the many profiles of the survey. When plotted on a potential temperature salinity diagram (Figure 1-1), the linear rela-

tionship in each layer is strikingly similar to the layer evolution observed in laboratory salt finger experiments (Lambert and Demenkow, 1972). Experiments and observations suggest that the centimeter-scale physics of the salt fingers are likely to be the dominate source of flux convergence which controls the relationship of temperature and salinity in the layers throughout the region. McDougall (1991) sought to explain this relationship in the context of a one dimensional flux ratio balance. Using the new observations of SFTRE we modify McDougall's solution to find a consistent estimate of the salt finger flux ratio.

An important aspect of the experimental design of SFTRE was quantifying the variability of the layers during the experiment so that the estimate of vertical eddy diffusivity for salt, K_S, from the HRP dives during first and second cruise could be compared with the time-averaged K_S deduced from the tracer data during the intervening 9 months. To this end, a new instrument, the WHOI Moored Profiler was deployed in February of 2001 from the *RV Oceanus* to record a time series of temperature, salinity and velocity profiles in the study region. The instrument was expected to operate for nine months until November when it was recovered. Normally capable of making over one million linear meters of profile observations, the instrument stopped due to a programming error after only 4.3 months. Nonetheless, the data collected provide a unique record of the thermohaline staircase structure and the evolution of layer properties.

Our analysis of this previously unattainable time series applies the conceptual model developed by McDougall to find a consistent estimate of the flux ratio. We begin by reviewing the results of salt finger observations, theory and laboratory work which bear upon our study of salt finger behavior (Chapter two). Next, we describe the Moored Profiler data and determine the linear relationship of temperature and salinity within each layer. The slope of this linear relationship is used to write a quantitative statement of the ratio of heat flux convergence to salt flux convergence in each layer (Chapter three). In chapter four, following McDougall (1991), we examine the terms of the buoyancy flux ratio as a continuous function of depth and derive two models relating the observations in the previous chapter to the flux ratio predicted in Chapter two. Using our new observations, we discuss the two models of vertical salt flux structure in an attempt to find a description consistent with salt finger theory and McDougall's equation for buoyancy flux ratio.
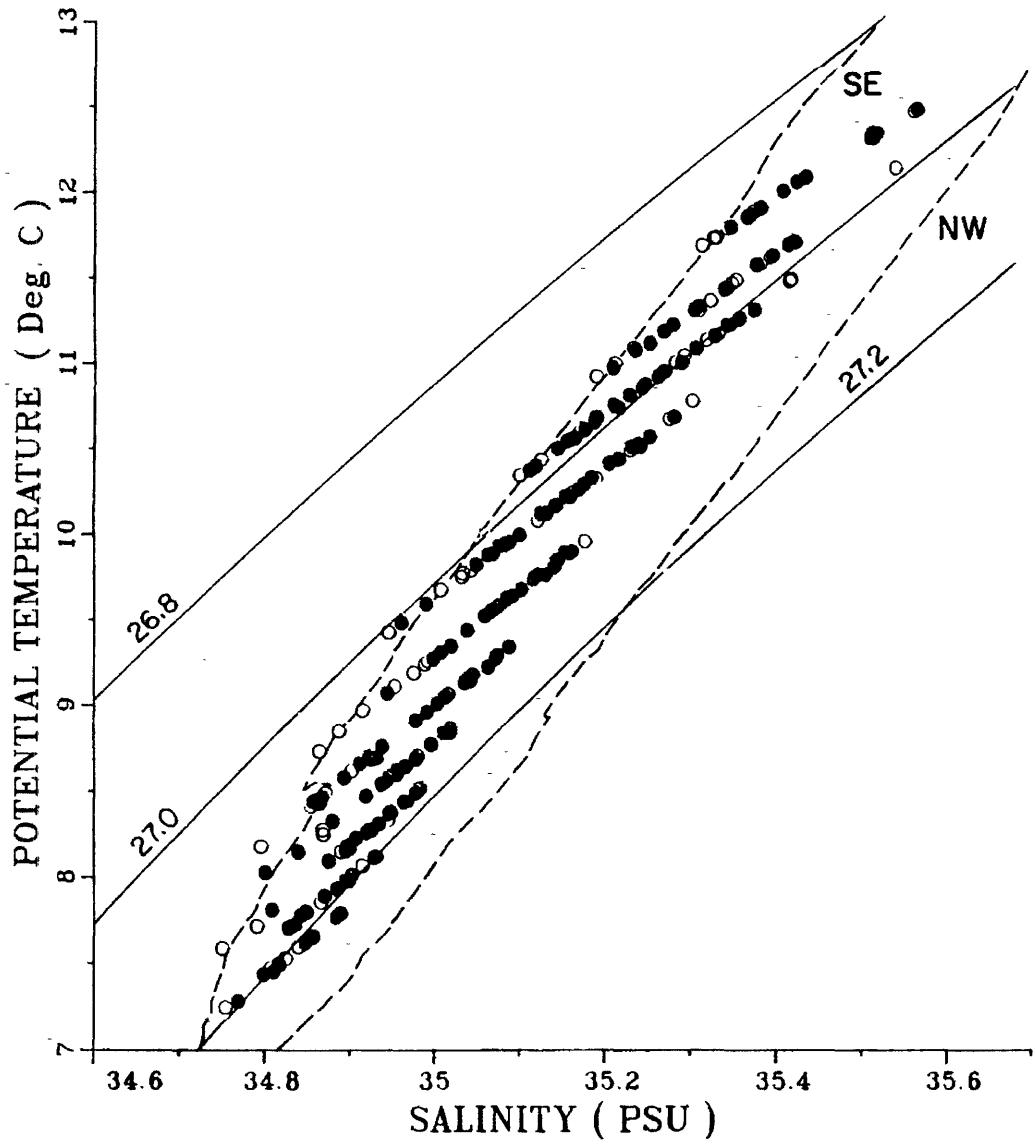
Figure 1-1: Θ—S diagram of the layers observed during the C-SALT spatial survey.
Published: Deep-Sea Research, Schmitt et al., 1987.

Chapter 2

Salt Fingers

Oceanic salt fingers are centimeter-scale plumes of rising and falling water which in cross section have the appearance of vertically interlocking fingers. The motion of the plumes is a special case of convective mechanical instability driven by the differential diffusion of heat and salt. The narrow aspect ratio of the plumes allows fast lateral diffusion of heat between plumes, effectively short circuiting the advective vertical flux of heat, but not salt, by the motion of the fingers. The molecular diffusivity of heat is greater then that of salt, $\kappa_T > \kappa_S$. The differential molecular diffusivity at small scales in growing salt fingers causes a reversal of the inequality for the large scale vertical eddy diffusivity where, $\mathbf{K_S} > \mathbf{K_T}$.

2.1 Observations of Salt Fingers

Salt fingers occur in the ocean in many places where a stable stratification of warm salty water overlies cold fresh water. The extent to which these gradients compensate is measured by the density ratio, $\mathcal{R}_\rho = (\alpha\theta_z)(\beta S_z)^{-1}$, with $\alpha = -\frac{1}{\rho_0}\frac{\partial\rho}{\partial\theta}$ and $\beta = \frac{1}{\rho_0}\frac{\partial\rho}{\partial S}$. The condition for linear unstable salt finger modes is $1 < \mathcal{R}_\rho < \frac{\kappa_T}{\kappa_S} \approx 100$, where the ratio of the molecular diffusivities is the Lewis number. Direct observations of salt fingers are consistent with the fastest growing mode of linear theory (Schmitt 2003). Images of oceanic salt fingers captured using an optical shadowgraph (Williams, 1974) support the towed microstructure data which has a dominant horizontal wavelength of 5-6 centimeters in agreement with theory (Magnell, 1973; Marmorino et al., 1987). In ocean observations and analogous laboratory experiments salt fingers are not ubiquitous in the water column but occur in thin interfaces. These interfaces are O[1 m] thick regions of high vertical gradient, separated by broad homogenous layers 10-20 meters thick. A sequence of such horizontal layers separated by steps of temperature and salinity at the salt finger interfaces create the characteristic thermohaline staircase often observed in CTD profiles. While the linear salt finger theory allows growing modes at high density ratio, staircase layers and distinctive microstructure are only observed at density
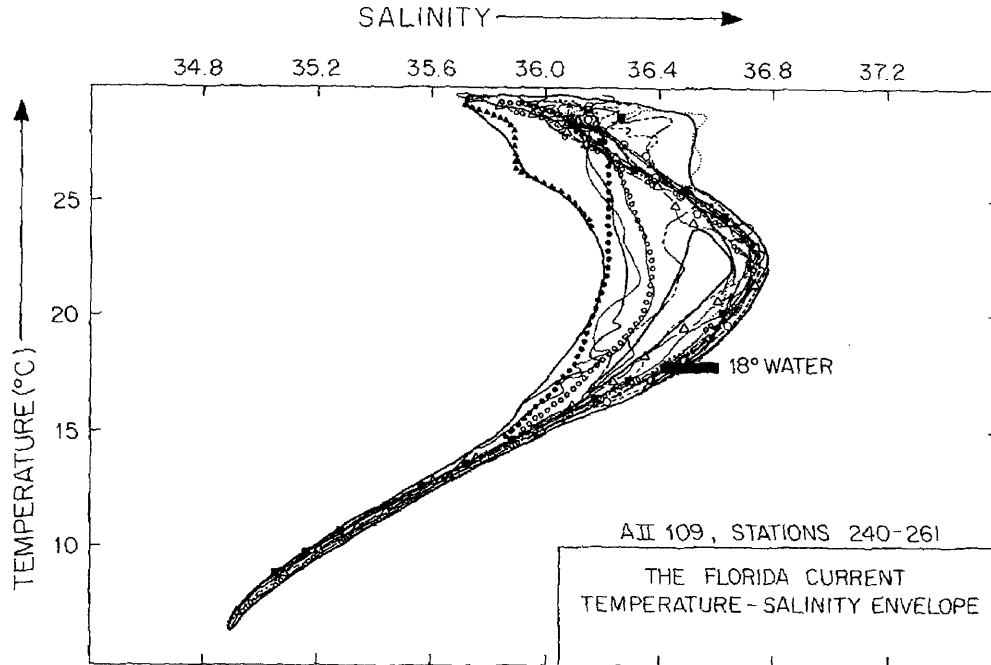
Figure 2-1: The temperature-salinity envelope of the *Florida Strait* waters. Published: Bulletin of Marine Science, Schmitz et al., 1993

ratios less than two where the salt finger growth rates can compete with mechanical turbulence supported by the ocean's shear and strain.

2.2 Water Mass Conversion

The subtropical central waters all have the necessary sense of stratification, warm salty water over cold fresh water, required to support salt fingers, but the most distinctive salt finger structures occur in regions of low density ratio $\mathcal{R}_\rho \lesssim 1.7$. There are many examples of small intrusions with low density ratio near strong fronts and eddies, but the signature, *salt finger staircases* occur where shear rotates large scale lateral gradients of temperature and salinity into the vertical. Arguably, the most important water mass conversion in which salt fingering have been implicated occurs in the western tropical North Atlantic where salinity maximum, Subtropical Under Water, flows west as part of the North Atlantic gyre, while beneath it, Antarctic Intermediate Water which crossed the equator, flows north. This superposition creates a region several hundred meters thick and thousands of square kilometers in area which is highly favorable to salt fingers. The absolute gradients of temperature and salinity are large and the density ratio is low resulting in large fluxes of salt between these water masses before they reach the Florida Current

on their way north to close the Atlantic mass balance across 24° North. Schmitz, Luyten, and Schmitt (1993) analyze the water masses of the Florida Current defining the potential temperature-salinity (θ–S) envelope of the waters in this narrow strait (Figure 2-1). Near the bottom, the coldest waters of the strait are 7-12° C. The envelope of temperature and salinity for this water is narrow. Its salinity is intermediate in the same temperature range between the dense, saline water of the Eastern North Atlantic on 24 °N (Figure 2-2), and the light, fresh water of the South Atlantic on 53°W (Figure 2-3). Further evidence from the oxygen content of this water suggests that it is in fact the South Atlantic water which has become saltier to create the observed θ–S envelope of the Florida Current. This interpretation requires a strong diabatic mixing process to increase the salinity but not the temperature of the South Atlantic water.

2.3 Salt Finger Flux Ratio

The buoyancy frequency (Equation 2.1) of the ocean is generally positive such that turbulent vertical mixing processes are a sink in the turbulent kinetic energy budget, raising the available potential energy of the ocean. Salt fingers are different. The vertical density gradient may be separated, using a linear equation of state, into the thermal and haline contribution (Equation 2.3). We are concerned with a mean state where the contributions oppose one another. Where both gradients are positive (upward vertical) the difference of their contribution to buoyancy is less than the absolute value of either component. In this context it is clear how the density ratio measures the extent to which the gradients of temperature and salinity compensate. As the density ratio approaches one, the magnitude of the buoyancy frequency (proportional to $[\mathcal{R}_\rho - 1]$) approaches zero. Salt fingers occur at low density ratio (near one) where the water column is sufficiently top heavy with salt for the efficient release of this potential energy.

$$\mathcal{N}^2 = -\frac{g}{\rho_0}\left(\frac{\partial \rho}{\partial z}\right) \tag{2.1}$$

$$\rho = \rho_0(T_0, S_0)\left[1 - \alpha(T - T_0) + \beta(S - S_0)\right] \tag{2.2}$$

$$\mathcal{N}^2 = -g\left[-\alpha\frac{\partial(T - T_0)}{\partial z} + \beta\frac{\partial(S - S_0)}{\partial z}\right] \tag{2.3}$$

$$\mathcal{N}^2 = g\left[\mathcal{R}_\rho - 1\right]\left(\beta\frac{\partial(S - S_0)}{\partial z}\right) \tag{2.4}$$

The buoyancy flux due to turbulent mixing is typically parameterized using an eddy diffusivity, K_b acting on the mean vertical density gradient (Equation 2.6). The assumption of equal mixing of heat and salt due to turbulence results in a down gradient density flux regardless of the density ratio. However, a sufficiently different vertical eddy diffusivity of heat and salt could release potential energy

21
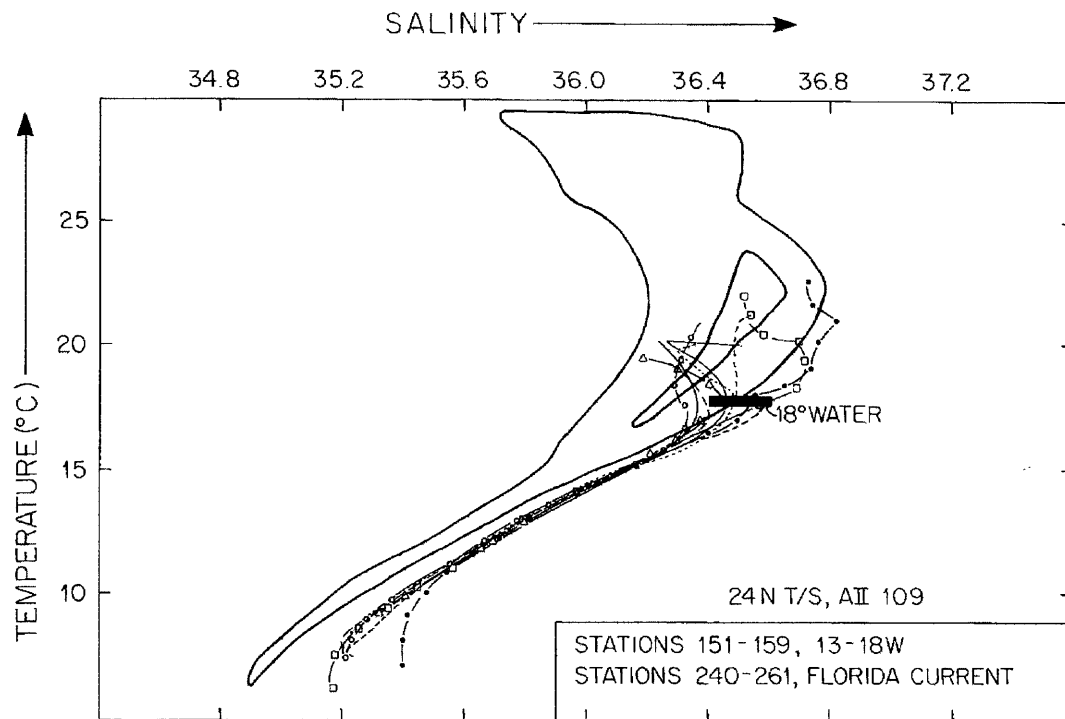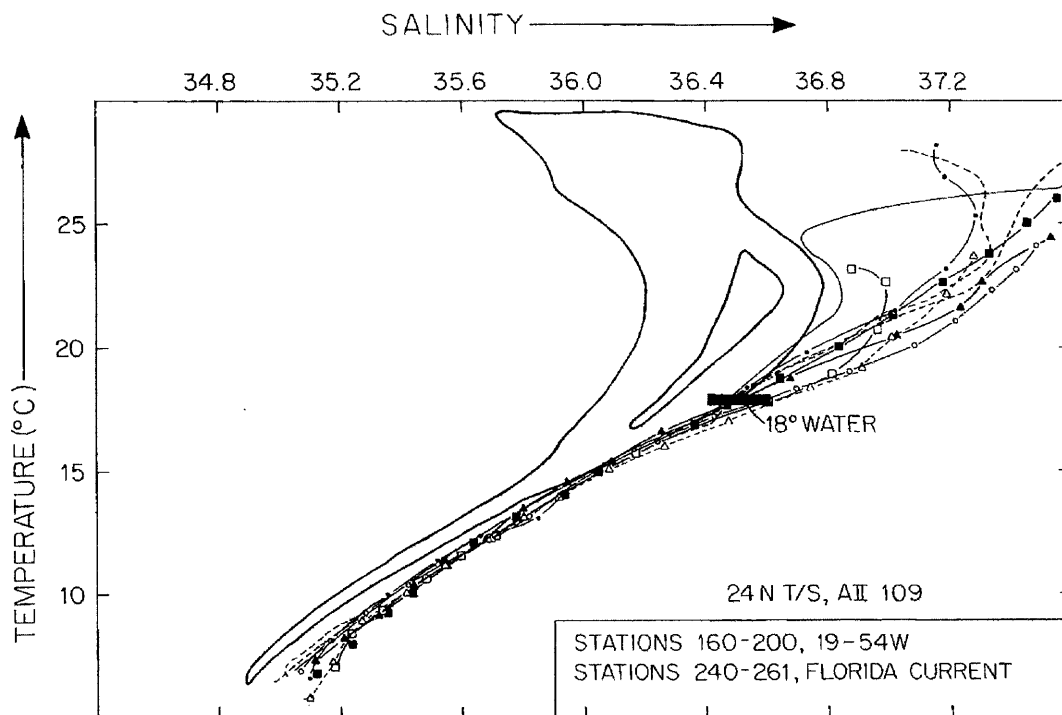
Figure 3a.

Figure 2-2: The temperature and salinity of the waters of the eastern Atlantic on 24°N. Published Bulletin of Marine Science, Schmitz et al., 1993

SALINITY

34.8   35.2   35.6   36.0   36.4   36.8   37.2

TEMPERATURE (°C)

25

20

15

10

18° WATER

STATIONS 212-228, 52W, 6.5-11.5N, Oc133
STATIONS 240-261, FLORIDA CURRENT, AII 109

Figure 4a.

SALINITY

34.8   35.2   35.6   36.0   36.4   36.8   37.2

TEMPERATURE (°C)

25

20

15

10

18° WATER

STATIONS 230-234, 52W, 12.5-14.5N, Oc133
STATIONS 240-261, FLORIDA CURRENT, AII 109
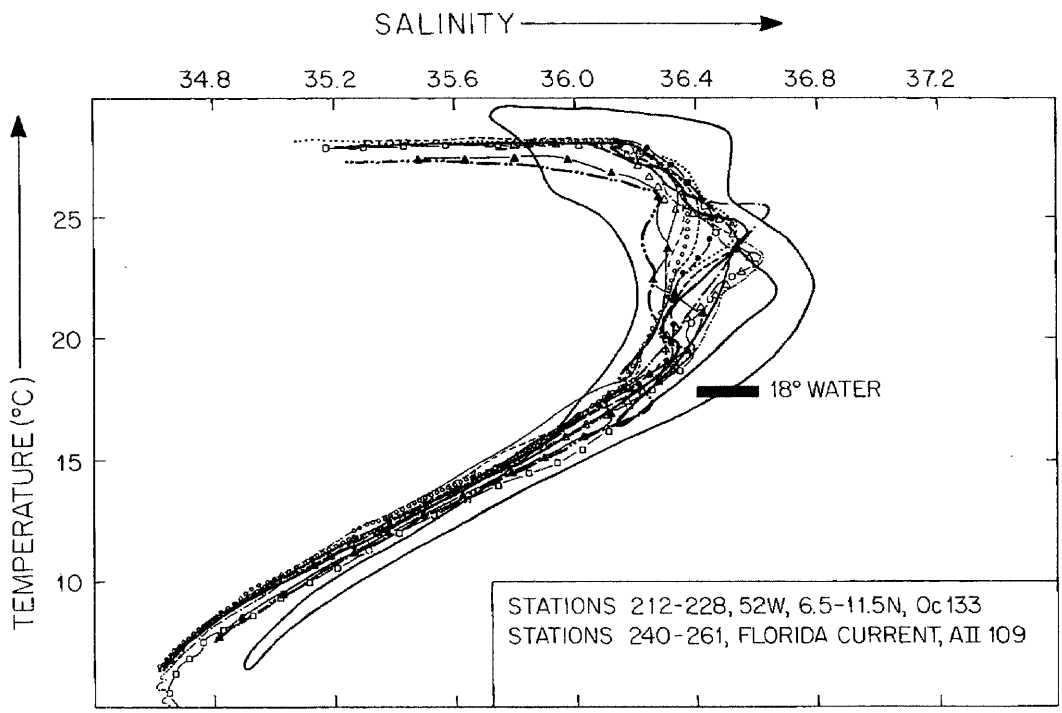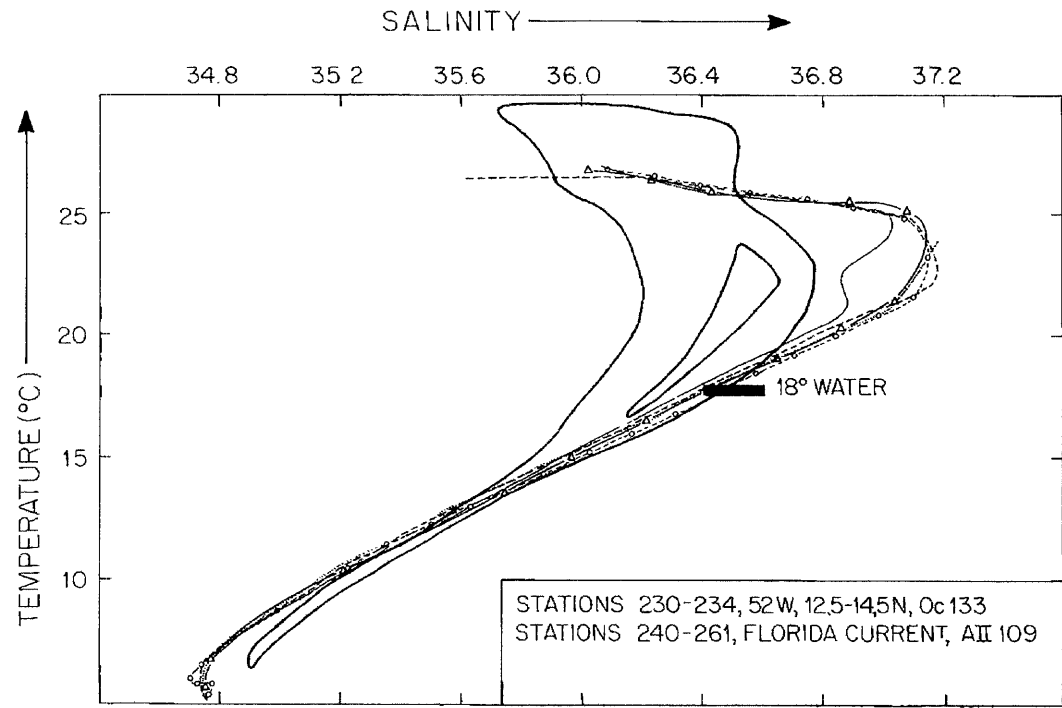
Figure 2-3: The temperature and salinity of water on the line 53°W. The salinity of the water in the Florida Straight below the 12° C isotherm has increased in the transit from 53°W, steepening the θ–S curve. These changes are consistent with vertical mixing due to salt fingers. Published Bulletin of Marine Science, Schmitz et al., 1993

in the unstable, haline component of the stratification (Equation 2.8). The difference between the molecular diffusivity of heat and of salt allow for just such an instability to occur: salt fingering. Analogous in form to the density ratio, the heat/salt buoyancy flux ratio, γ (Equation 2.5) described in Stern (1975), measures the efficiency of the short circuit mechanism by which salt fingers make use of the available potential energy in the haline stratification. This potential energy is a source in the turbulent kinetic energy equation if and only if ($\gamma < 1$) such that the buoyancy flux changes direction because ($\frac{K_S}{K_T} > \mathcal{R}_\rho$).

$$\gamma \equiv \frac{\alpha < \overline{w'T'} >}{\beta < \overline{w'S'} >} \tag{2.5}$$

$$\mathcal{F}^b = -\mathbf{K_b} \left[\mathcal{N}^2 \right] / g \tag{2.6}$$

$$\mathcal{F}^b = \left[-\alpha \mathbf{K_T} \frac{\partial (T - T_0)}{\partial z} + \beta \mathbf{K_S} \frac{\partial (S - S_0)}{\partial z} \right] \tag{2.7}$$

$$\mathcal{F}^b = [1 - \gamma] \left(\beta \mathbf{K_S} \frac{\partial (S - S_0)}{\partial z} \right) \tag{2.8}$$

$$\gamma = \frac{\alpha \mathbf{K_T} \frac{\partial (T - T_0)}{\partial z}}{\beta \mathbf{K_S} \frac{\partial (S - S_0)}{\partial z}} \tag{2.9}$$

$$\gamma = \frac{\mathbf{K_T}}{\mathbf{K_S}} \mathcal{R}_\rho \tag{2.10}$$

The condition, $\gamma < 1$, implies that the double-diffusive buoyancy flux of salt is larger than that of heat. The flux of density is therefore up-gradient which acts to enhance density gradients via a negative buoyancy diffusivity. Given this necessary condition for salt finger growth, salt fingers cause a buoyancy flux convergence on perturbations to the stratification. This maintains the steps of the staircase against the smoothing effects of turbulent mixing (Schmitt, 2003). The variation of eddy diffusivity, and therefore the flux ratio with density ratio has recently been implicated as the driving mechanism in the formation of staircase layers. Analytic models provide a mechanistic explanation of the behavior observed in numerical simulations where flux convergence on density ratio perturbations leads to step formation from a uniform stratification (Radko, 2003).

The salt finger literature addressing the dependence of the buoyancy flux ratio on the density ratio is extensive. Stern (1975) derived the fastest growing linear normal mode for viscous salt fingers. At low density ratio (near one), $\gamma = \mathcal{R}_\rho - \sqrt{\mathcal{R}_\rho^2 - \mathcal{R}_\rho}$ which is the asymptotic limit of the full similarity solution derived by Schmitt (1979). The relationship of the fastest growing mode to the flux ratio is set by the competing effects of the Prandtl number and the Lewis number as the aspect ratio of the fingers change. These are constants in the ocean (Prandtl number is ~ 7 while the Lewis number is ~ 100) so that the aspect ratio, and associated flux ratio, of the fastest growing mode is determined by the density ratio. This re-

24

lationship has been tested in the laboratory by numerous experiments (Figure 2-4). St.Laurent and Schmitt (1999) recently published an estimate of flux ratio variability with density ratio from measurements of ocean microstructure. The body of evidence summarized in figure 2-4 suggests that the flux ratio does in fact vary with density ratio. While the conglomeration of data scatters over a large range of density ratio, independently three of the data sets shown suggest a correlation of flux ratio and density ratio. I argue that the scatter between these experiments might be accounted for by an unknown parameter which might be fixed in the experiments of each researcher but not normalized between the separate estimates shown in the figure. For simplicity we will retreat from the laboratory and experimental estimates of the flux ratio and use the analytic form derived by Stern for the fastest growing finger mode to model the flux ratio $\gamma = \mathcal{R}_\rho - \sqrt{\mathcal{R}_\rho^2 - \mathcal{R}_\rho}$. This model estimates the flux ratio to be 0.6 for a density ratio of 1.6, which is roughly consistent with the mean flux ratio of the experimental work. Note that this model, though linear, is a valid finite amplitude similarity solution to the boussinesq equations in a region of uniform gradients (Schmitt, 1979)

2.4 Salt finger Flux Ratio measurements

In the laboratory, salt finger tank experiments make use of the simple boundary conditions to measure the salt finger flux ratio. By studying salt fingers on an interface between two thick layers in a tank, the measurement of the average flux of heat and salt, $< \overline{w'T'} >$ and $< \overline{w'S'} >$, becomes a straightforward measurement of the temperature and salinity of the layers over time. Given a well insulated tank which allows no flux of heat or salt through the walls, changes in temperature and salinity must be due to the double diffusive flux across the interface. This not only eliminates the need to measure a turbulent correlation but also leads to the flux ratio being independent of the volume of the layer, $\gamma = (\alpha \frac{\partial T}{\partial t})/(\beta \frac{\partial S}{\partial t})$. The flux ratio is the time rate of change of temperature divided by the time rate of change of salinity (Figure 2-5). The actual heat content and mass of salt are not at issue such that the volume of the layer divides out of the equation and does not enter the expression for the flux ratio. The ratio can then be measured by taking the slope of points in a temperature salinity time series from a layer (Lambert and Demenkow, 1972). The critical point in this analysis is that we have implicitly assumed the flux across the interface is equal to the flux divergence within the layer due to the no-flux boundary condition at the tank walls.

McDougall (1981) pointed out several problems with the assumptions of this model due to the nonlinear equation of state (e.g. it relies on a Boussinesq conservation of volume). The leading-order correction in oceanic salt fingers is due to interfacial migration. In the laboratory this phenomena is observed to always cause an upward movement of the interface. The flux ratio of the upper layer
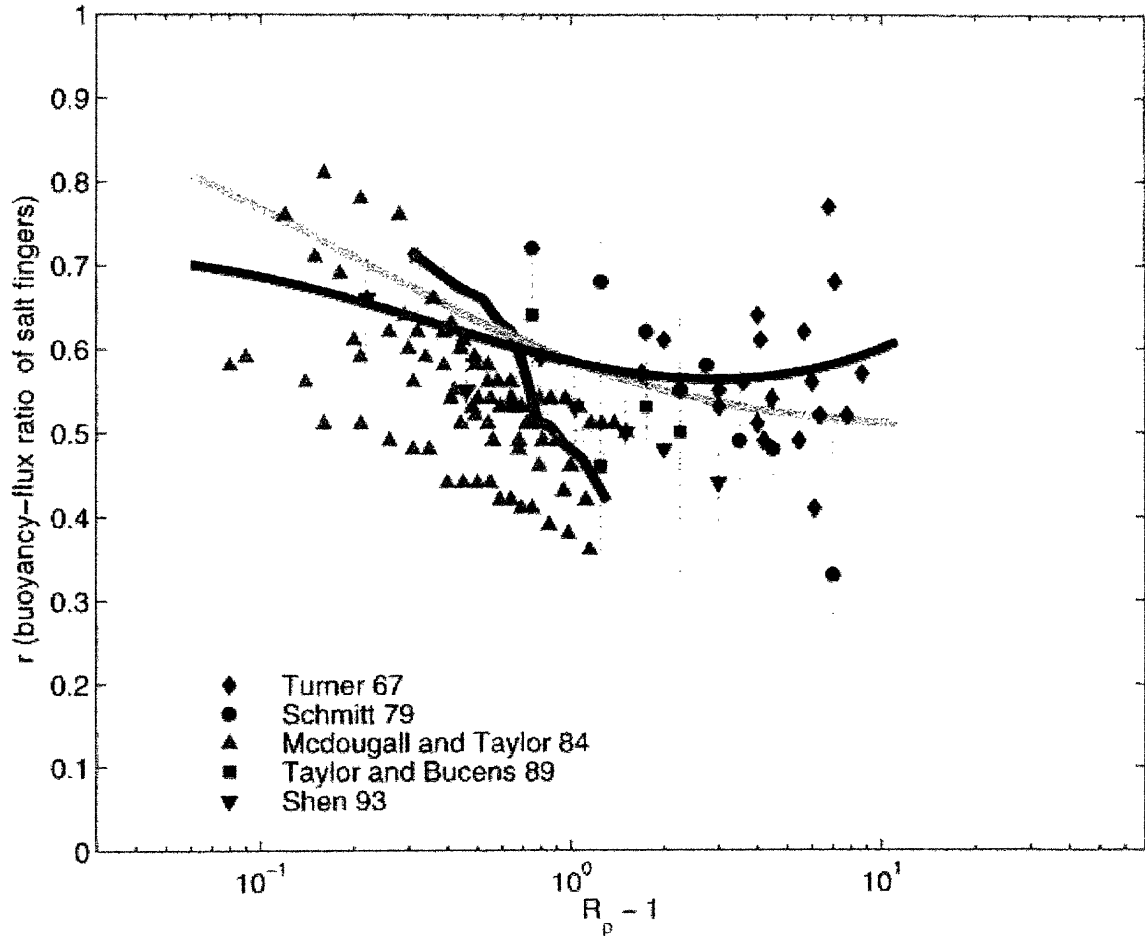
Figure 2-4: Summery of observational and theoretical flux ratio estimates as a function of $\log(\mathcal{R}_\rho - 1)$: The laboratory experiments are listed in the legend. The observational estimates derived from HRP microstructure measurements comprise the steeper black curve. Stern's asymptotic solution is shown in gray in comparison with the data and Schmitt's similarity solution for finite amplitude in black. Published: JPO 1999, St.Laurent and Schmitt
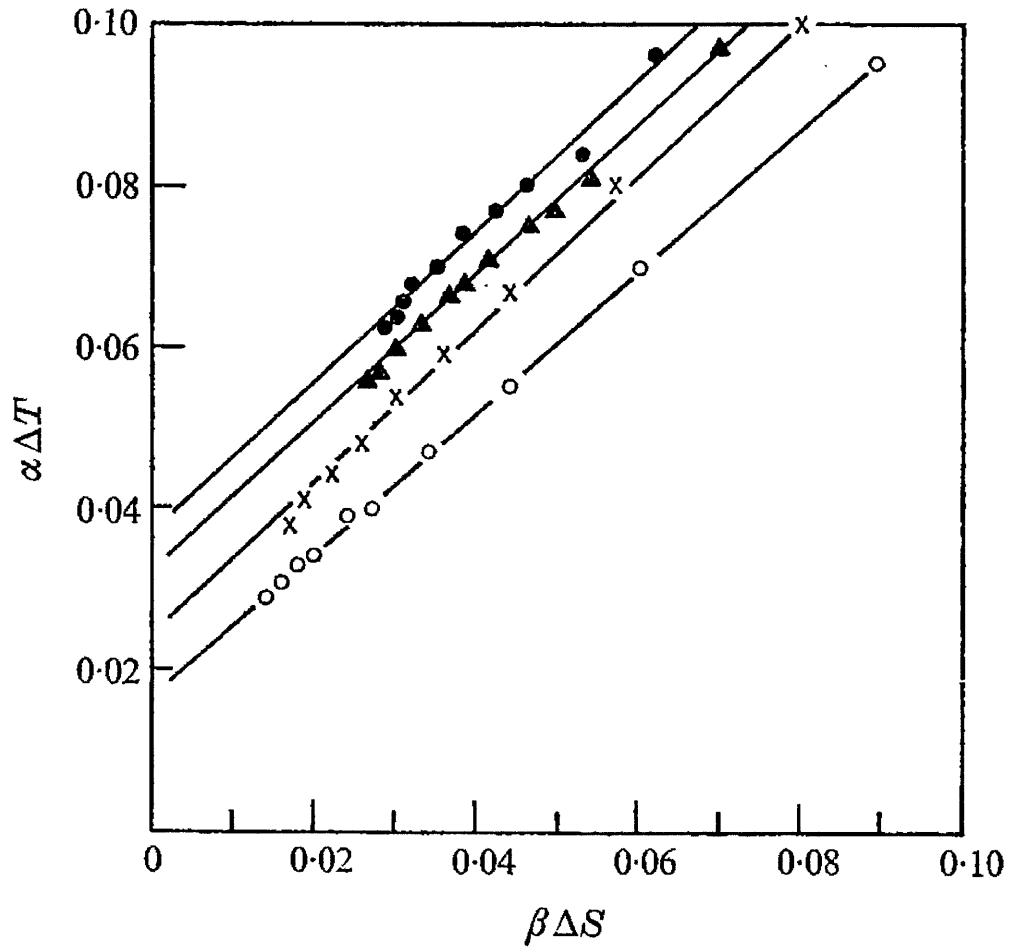
Figure 2-5: Observations of temperature and salinity difference between the upper and lower layer of laboratory salt finger experiments conducted by Lambert and Demenkow. Observations begin in the upper right as the initial condition runs down to the lower left. The slope of data from each experiment is the estimated flux ratio. Published: Journal of Fluid Mechanics 1972, Lambert and Demenkow.

will remain unaffected by this downward diapycnal velocity at the interface, but the lower layer will experience a flux of heat and salt proportional to ΔT and ΔS respectively. The observed temperature-salinity correlation in staircase layers of the CSALT data resemble the temperature salinity diagrams of Lambert and Demenkow's laboratory work. The similarity led McDougall (1991) to find a relationship, based on his more careful consideration of the non-linear equation of state, between the flux ratio and the correlation or layer slope in the CSALT temperature salinity diagram. Using a time series of temperature and salinity in the thermohaline staircase layers East of Barbados from SFTRE, we seek a more nuanced analysis of the implications of the layer slope observed in the time series, similar to that in CSALT. Applying our understanding of the salt finger flux ratio in conjunction with the new Moored Profiler data we will test McDougall's assumptions and conclusions and propose a new model for the profile of the salt flux which better accommodates our understanding of the small and large scale processes involved.

Chapter 3

Observations of Temperature and Salinity from a Moored Profiler

Salt finger fluxes are a mechanism for ocean mixing, but are difficult to measure directly. Salt fingers act on the meso-scale and large-scale properties of the ocean, and in this way we are able to indirectly observe their effects. We will assume here that if salt finger fluxes are the leading order term in the evolution of the thermocline and halocline, then they maintain a thermohaline staircase. Conversely, we will assume that if a thermohaline staircase structure is observed, it necessarily implies that salt fingering is the primary agent determining that structure in the absence of competing physical processes. Therefore, the striking layers of temperature and salinity in the SFTRE Moored Profiler data present an opportunity to study the impact of salt fingers as an isolated process.

The staircase structure of the thermocline in the ocean east of Barbados is an ideal case study for testing salt finger theory. Understanding such a beautiful self organizing physical phenomena is intrinsically valuable, but we may also extrapolate our findings to hypothesize about the local and global significance of the salt flux through the staircase to the ocean circulation. Beyond the handful of regions which exhibit a such a large thermohaline staircase, the central waters of the subtropics have a low density ratio favorable to generating mixing by salt fingering. While these vast regions are a more complicated mixing environment in which fluxes due to double diffusion are only one of many processes involved, this study makes a contribution to delineating the relative contribution of salt fingers to mixing in the greater world ocean.

3.1 Data and Instrumentation

The WHOI Moored Profiler (Toole et al., 1999; Doherty et al., 1999) deployed near the center of the SFTRE study region at 13°N 55°W (Figure 3-1) repeatedly profiled the same location recording temperature, salinity, pressure and velocity. The in-
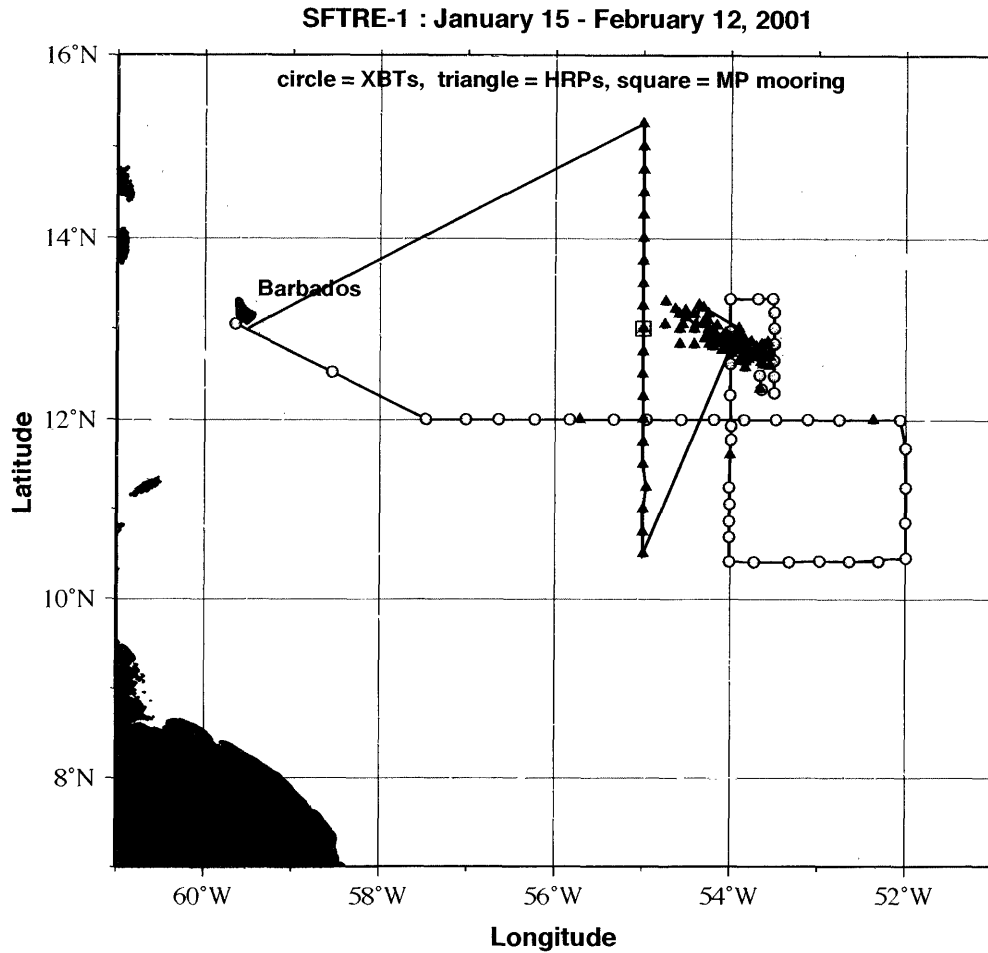
Figure 3-1: Station positions from the first cruise of the Salt Finger Tracer Release Experiment. The figure details the location of High Resolution Profiler, expendable bathythermograph, and Moored Profiler stations. The Moored Profiler was located at 13°N 55°W, while the SF_6 tracer was injected to the South and West at 12°45′ N 53° 45′ W in a layer on the 1027.045 isopycnal. Figure contributed by Ellyn Montgomery.

strument made 775 such profiles of the water column between 100 and 700 meters depth over 129 days.

Raw data from each profile is processed and binned to a two-decibar grid. One-way profiles, which take about an hour to complete, were repeated approximately every four hours. Sample intervals at each depth are asymmetric due to the alternating direction of motion. The four hour time series interval is significantly modified by the finite time required for the instrument to make a profile. The 582 decibar bin is the special depth at which the time series interval is equal to its average and uniformly four hours to within a few seconds for all 775 profiles.

Temperature and salinity are measured using a Falmouth Scientific Inc. (FSI) Excell Micro CTD. After processing, we expect the observations to have a precision better then 0.005 for both temperature and salinity. The velocity is measured using an FSI 3D-Acoustic Current Meter designed for the Moored Profiler. We expect the processed velocity observations to be accurate within 5%. The observation noise is somewhat higher than expected from instrument calibrations of the CTD and ACM. The autonomous profiling capability comes at a cost associated with subjecting the instrumentation to a rapidly varying temperature field and strong vibrations. As with any measurement, we fight at the margin to recover as many significant figures as possible. The benefits of the Moored Profiler, capturing a unique time series of fine-scale profiles at this location using a single set of instruments, far outweigh the cost of the noise level which has continued to decrease as the instrument design improves.

3.2   Observations of the Staircase

The temperature and salinity data from the SFTRE Moored Profiler capture the evolution of the staircase over four months. The steps, characteristic of double diffusion, are evident in all of the acquired profiles, though their clarity does vary over time. A particularly sharp example, shown in figure 3-2, has 15 visible layers which range from 4 to 40 meters thick. The potential temperature difference between layers is as large as 1°C. The salinity difference is remarkably well correlated with the temperature difference, fixing the density ratio near 1.6 throughout the staircase. Internally, the layers are well mixed, presumably by the buoyancy fluxes across the interfaces at top and bottom of each layer. Temperature-salinity inversions are relatively rare within the layers during the time series.

The motion of the internal wave field makes it inconvenient to work with the time variability of the layers using the pressure gridded data. The temperature and salinity of the layers change much less between profiles than does their depth. By making a scatter plot (Figure 3-3 a) of the potential temperature vs time the continuity of the layers over the four month time series becomes apparent. Conformal mapping of pressure-binned-data on to temperature coordinates stretches sharp gradients in a profile while collapsing each homogeneous layer to a single

31
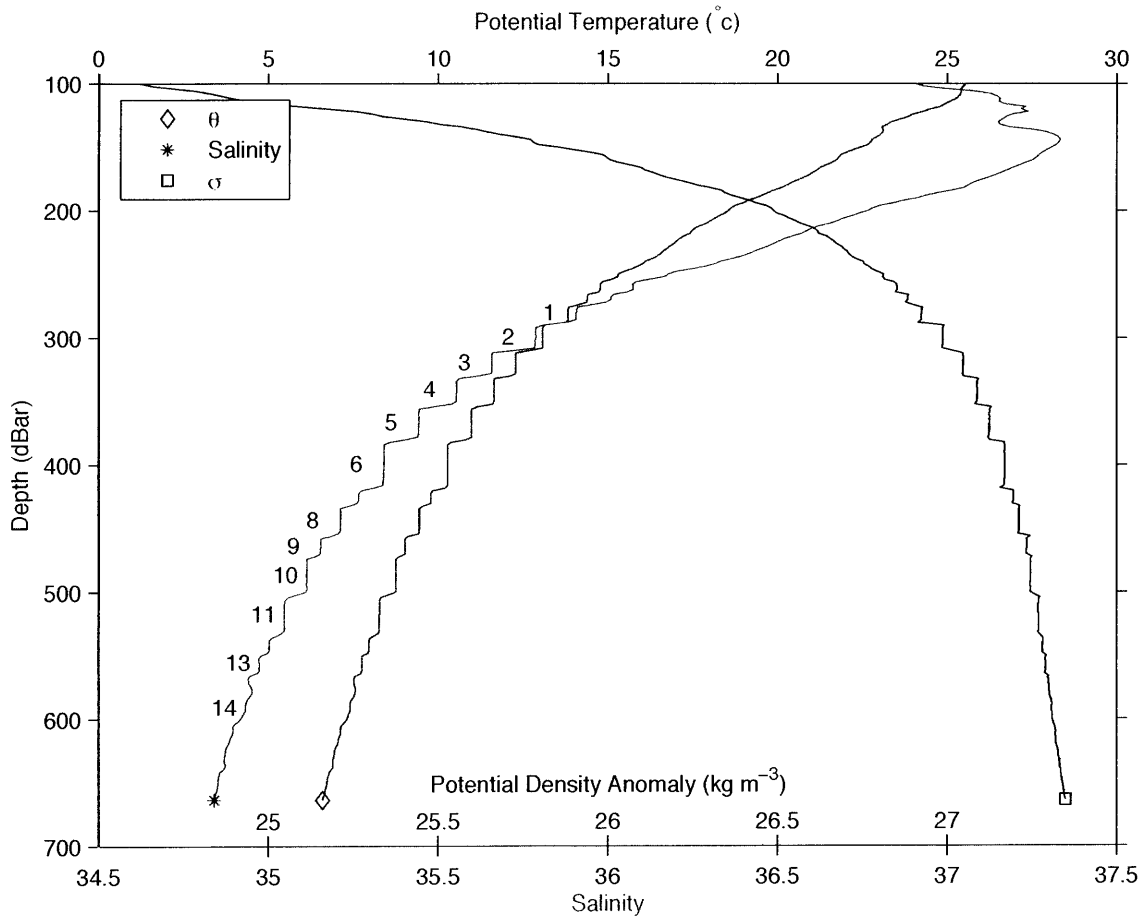
Figure 3-2: A single profile from the mooring showing the thermocline and the staircase in potential temperature, salinity and potential density anomaly. Layers which are identifiable in this profile have been numbered for comparison with other figures throughout this chapter.

point in temperature. The discrete uniform vertical spacing of the observations is fundamental to this approach. The visually dense clusters of data points manifest the thick layers which occupy several two-decibar bins in each profile. The visually sparse regions between layers are the thin, sharp gradients where salt fingering occurs. The amount of scatter in the interfaces is a representation of their thickness, or equivalently the magnitude of the vertical gradient. This temporal variability of the interfaces is quantified by the layer index (Figure 3-3 b) which measures the percentage of two-decibar observations between fixed depths with a gradient less than $(1°C/100m)$. As expected from this definition, the index is strongly correlated with the clarity of the layers in the scatter plot. In spite of the considerable variability of the layer index and several abrupt changes in layer temperature of order $1°C$ during the time series, many of layers are continuous over the four months of the time series. The spatial continuity of layers, even near sharp fronts, was one of the most surprising results of the potential temperature-salinity diagram from the C-SALT survey, and is confirmed by the time series from SFTRE.

3.3 The Potential Temperature-Salinity Diagram

The slope of a line connecting two observations on the $\Theta-S$ diagram is the ratio of the gradient of temperature to the gradient of salinity between the two observations in space or time. Lambert and Demenkow (1972) used this property to determine the ratio of the rate of change of temperature and salinity in their laboratory experiments. The $\Theta-S$ diagram of ocean profiles has also been used by Schmitt (1981) to show that the central waters of the ocean are, to a good approximation, regions of constant density ratio and different from a linear mixing line. The density ratio is the scaled slope between two $\Theta-S$ observations in a profile, equivalent to the ratio of the vertical buoyancy gradients as defined in Chapter two.

The potential temperature-salinity diagram has the same effect of stretching gradients noted in the temperature scatter plot such that the layers of the salt finger staircase appear as dense clusters. The clusters found in the Moored Profiler data are linear, just like those in the $\Theta-S$ diagram from CSALT (Figure 1-1). Using the 218,304 observations of temperature and salinity from the Moored Profiler we can construct a discrete joint probability density function which highlights the clusters of data in the layers due to the large number of observations relative to the thin, sparse interfaces. Binning the data in $\Theta-S$ space to create a bivariate histogram of the observations (Figure 3-4), the high density of observations in the layers stand out clearly against the background clutter of observations which occur in the interfaces. The observations demonstrate that the ratio of the rate of the change of temperature to the rate of change of salinity in each layer is constant, throughout the range of temperature and salinity in each layer during the time series. We will define a layer statistically as a small region surrounding a linear fit (Figure 3-5) to

33
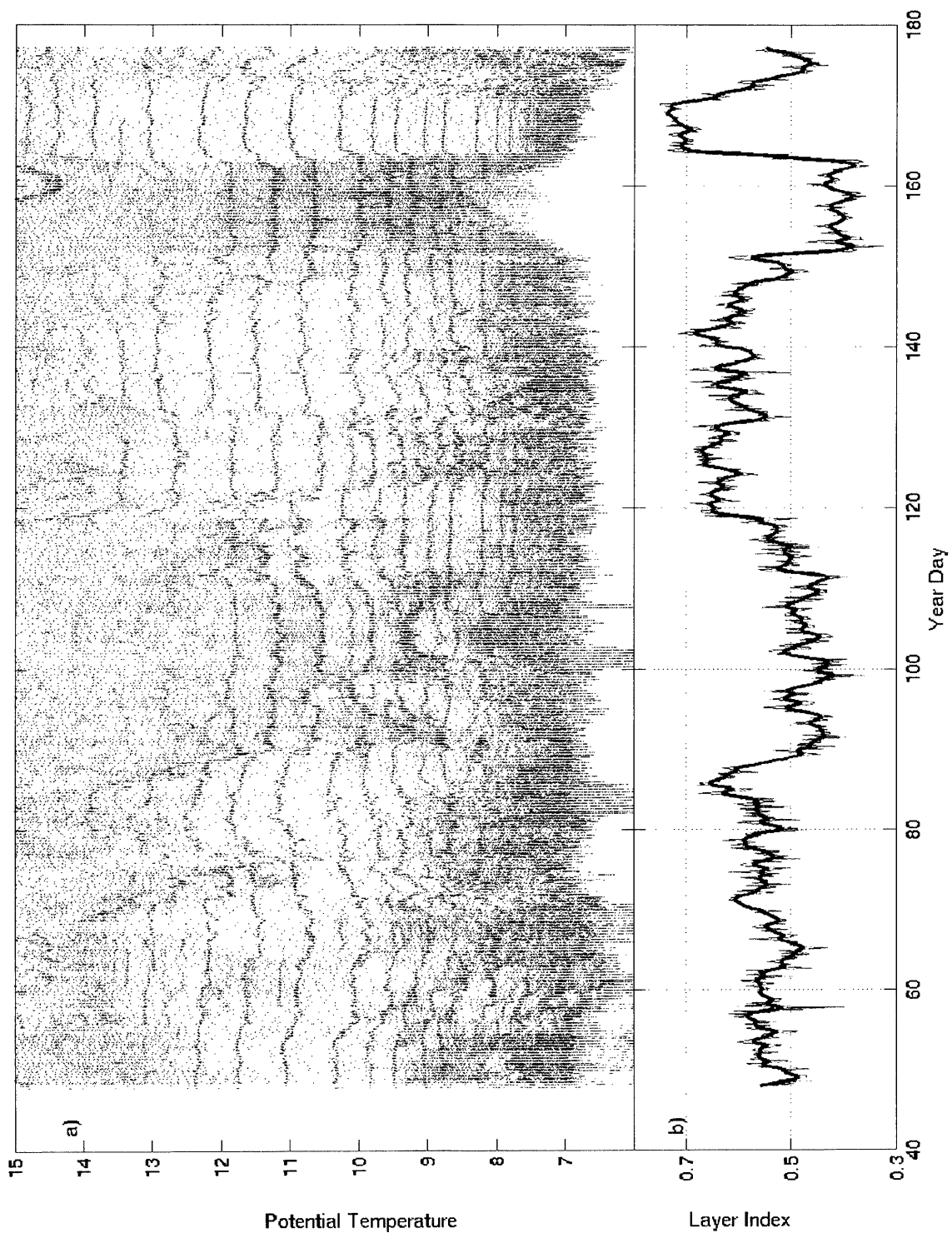
Figure 3-3: a) Scatter plot of the potential temperature in time during the 129 day Moored Profiler record. The y-axis has been limited to show only the lower thermocline and the staircase layers. b) Layer index is calculated by $Li = P\{| \frac{\Delta T}{\Delta Z} | < 0.01\}$. The raw layer index time series (blue) is shown with a low pass filter superposed (red). These figures are a time series of the layered structure of the staircase. Notice the relationship between the clarity of the layers in the scatter plot and the value of layer index.

34
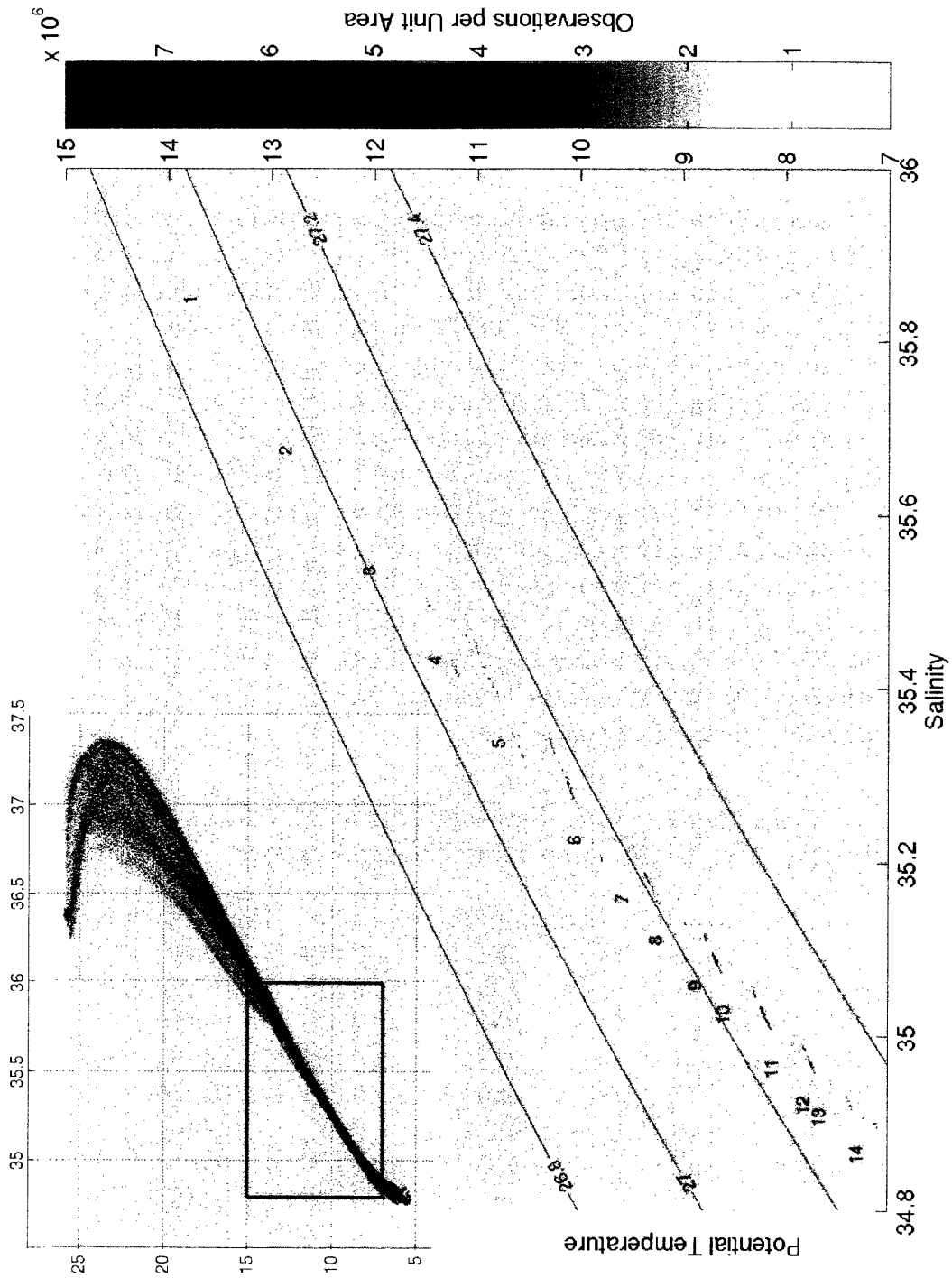
Figure 3-4: The Θ–S curve in the upper left is a scatter plot of all 218,304 observations. The distribution or density of these points in Θ–S space is binned to create the color scaled 2-dimensional histogram. The units of the color scale are given as observations per unit area of Θ–S space. Each observation is a sample of two meters of water column so that of the total 436,608 meters of water sampled during the time series, the color represents the volume of water observed at a particular temperature and salinity.

35

the layer-clusters of the Θ–S diagram. The orientation of these clusters or the layer slope, scaled by α/β, is referred to as $\mathcal{R}_L$.

3.4 Determining $\mathcal{R}_L$

Finding a linear relationship in data with pervasive background clutter is a difficult problem in statistics. I chose to use a simple working definition of a layer which incorporates information about both the temperature and the salinity in estimating the slope. Using the binned data of the histogram in figure 3-4, for each bin in salinity we find the temperature bin with the maximum number of data points (for each bin in salinity $x(i)$, find the temperature bin $y(j)$ in each layer which maximizes the probability density of the observations. For $z = pdf\{x, y\}$, find $y(j)$ such that $z\{x, y\} = \max[z\{y(j)\}\|_{x(i)}]$). On each layer this yields a series of points to which I fit a line in a simple least squares sense. The process removes the clutter from the interfaces. Observations which lie within a small range of temperature from the linear fit are defined to be in a layer. Based on this working definition of a layer we can identify 14 layers in the Moored Profiler data. The analysis provides two types of information about each layer. First we identify $\mathcal{R}_L$ and an associated error based on the statistics of the linear fit (Table 3.1), and second, a time series of temperature and salinity in each layer.

Table 3.1: Scaled layer temperature-salinity slope, $\mathcal{R}_L$, estimated using a linear fit to the temperature-salinity probability density maxima.

Layer #	Mean Depth (m)	$\mathcal{R}_L$	Error(1 std)
1	286	0.644	0.060
2	293	0.825	0.009
3	311	0.870	0.006
4	338	0.886	0.004
5	366	0.891	0.005
6	400	0.877	0.004
7	428	0.820	0.011
8	451	0.849	0.005
9	474	0.836	0.020
10	494	0.826	0.007
11	525	0.782	0.009
12	542	0.771	0.026
13	561	0.795	0.013
14	593	0.921	0.025

Using this definition, the layer property time series are discontinuous although the central layers are apparent in almost all profiles. An example of the resulting
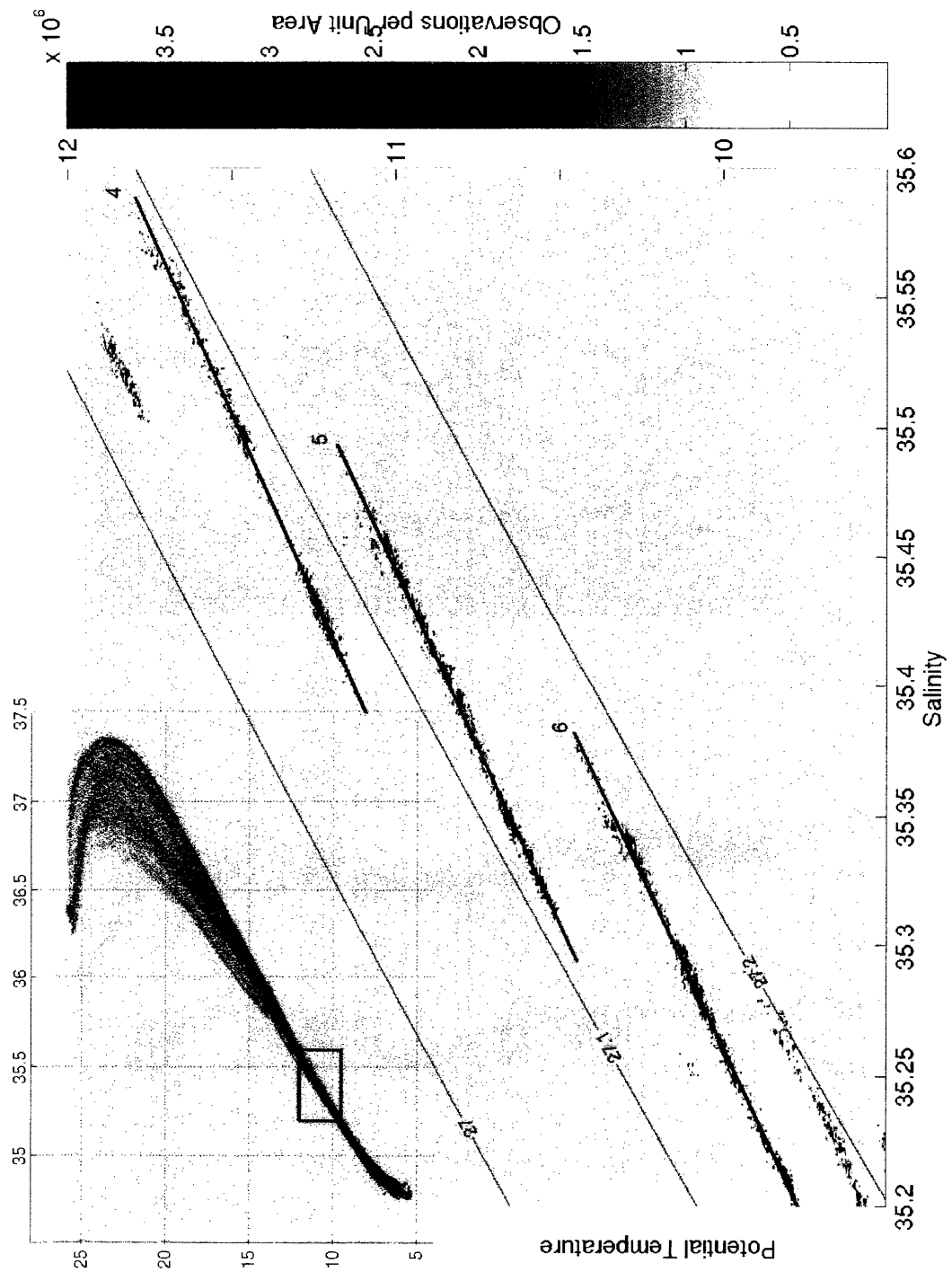
Figure 3-5: Zooming in on the previous figure, the results of a linear fit to three of the central layers are shown superposed on the observation-density color plot in potential temperature and salinity space.
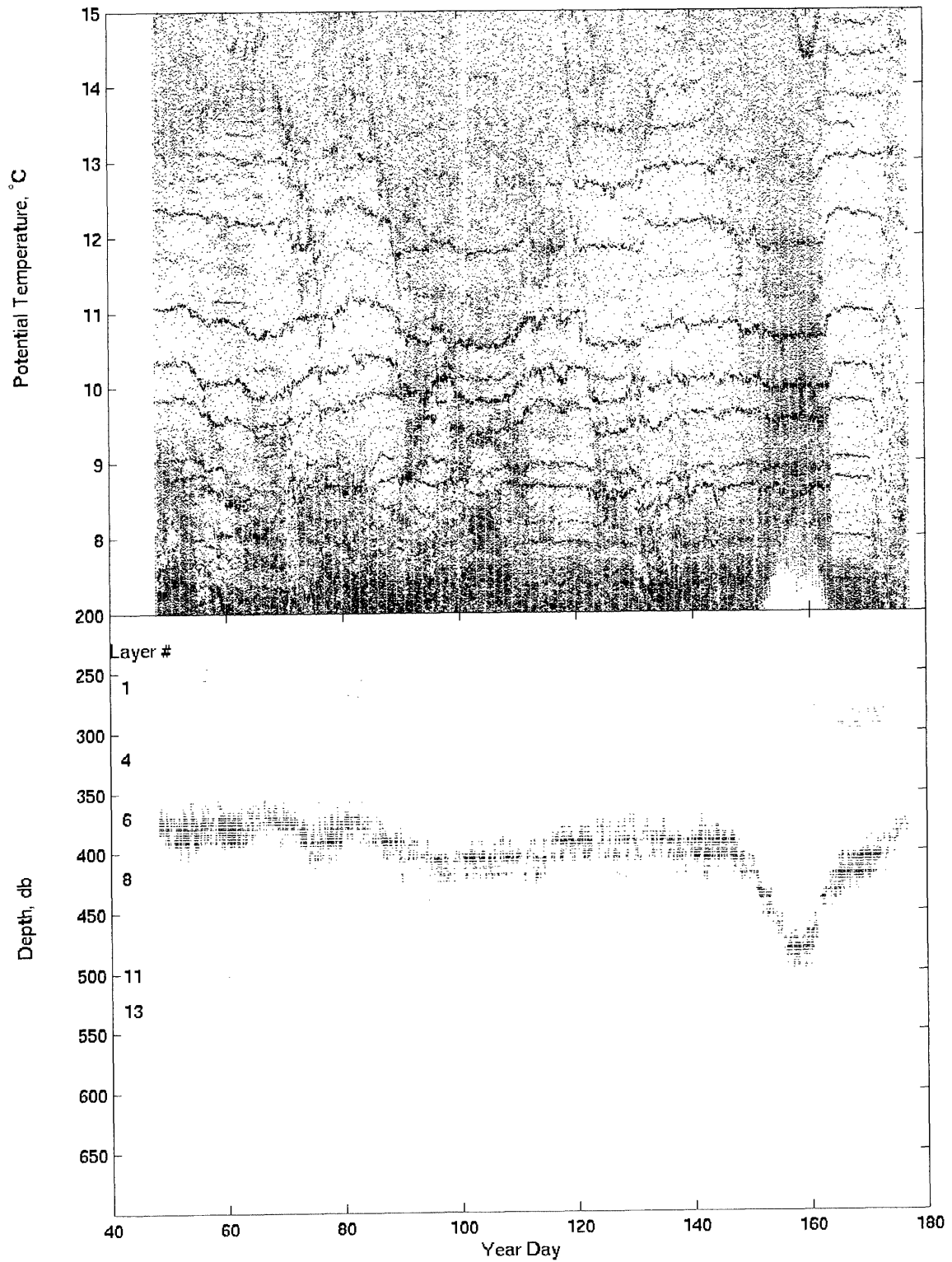
Figure 3-6: The time series of potential temperature (upper axes) and pressure (lower axes) for 6 of the 14 identified layers. These are numbered from top to bottom at the left hand side of the pressure scatter plot.

time series in pressure and temperature appears in figure 3-6. We are interested in the time average properties of the layers and the time average profile so that we may study the structure of the staircase in relation to $\mathcal{R}_\text{L}$. However, the statistics of layer depth shown in the pressure time series are highly skewed (the third moment is large) such that the mean and variance are a poor description. The time average layer depth provides a basis for comparing the vertical structure of layer properties but should be taken as indicative of the mean distance between layer centers, not the physical location of the layers.

The temperature and salinity difference between adjacent layers can also be calculated in any profile for which both layers can be identified by their Θ–S relationship. Before we can use the measurements to calculate the mean density ratio between layers we must clearly define what is meant by the *time-mean density ratio*. The expected value of a quotient of two dependent random variables is not the same of the ratio of their expected values. The pit-falls which await are evident in the ratio of independent normal random variables. The variance of such a ratio is not finite. The mean (Equation 3.2) and variance (Equation 3.3) of a quotient can be written as a Taylor expansion about the ratio of the mean values in terms of the variance and covariance of the numerator and denominator (Mood, Alexander and McFarlane, 1974). The mean value, μ of the buoyancy scaled potential temperature difference and buoyancy scaled salinity difference are, $\mu_{\Theta'} = \mathcal{E} [\alpha\Delta\Theta]$ and $\mu_{S'} = \mathcal{E} [\beta\Delta S]$ where we have used Θ' and S' as a short hand for the buoyancy scaled gradients. α and β are calculated at the mean salinity, temperature and pressure of the two layers at each time point. The variance and covariance of these variables are respectively:

$$\text{var} [\Theta'] = \mathcal{E} \left[(\alpha\Delta\Theta - \mu_{\Theta'})^2 \right]$$
$$\text{var} [S'] = \mathcal{E} \left[(\beta\Delta S - \mu_{S'})^2 \right]$$
$$\text{cov} [\Theta', S'] = \mathcal{E} \left[(\alpha\Delta\Theta - \mu_{\Theta'})(\beta\Delta S - \mu_{S'}) \right]$$

Using these terms we may write an approximate expression for the time mean and variance of the density ratio for each of the thirteen interfaces in the Moored Profiler data. The result is significantly different from other less rigorous approaches that were tested.

$$\mathcal{R}_\rho = \frac{\alpha\Delta\Theta}{\beta\Delta S} \tag{3.1}$$

$$\mathcal{E} [\mathcal{R}_\rho] \approx \frac{\mu_{\Theta'}}{\mu_{S'}} - \frac{1}{\mu_{S'}^2}\text{cov} [\Theta', S'] + \frac{\mu_{\Theta'}}{\mu_{S'}^3}\text{var} [S'] \tag{3.2}$$

$$\text{var} [\mathcal{R}_\rho] \approx \left(\frac{\mu_{\Theta'}}{\mu_{S'}}\right)^2 \left(\frac{\text{var} [\Theta']}{\mu_{\Theta'}^2} + \frac{\text{var} [S']}{\mu_{S'}^2} - \frac{2\text{cov} [\Theta', S']}{\mu_{\Theta'}\mu_{S'}}\right) \tag{3.3}$$

The results of the observational analysis are summarized in figure 3-7. To com-

pare the profile of time average quantities observed on the interfaces, such as density ratio, $\mathcal{R}_\rho$, with those observed in the layers, such as layer slope, $\mathcal{R}_L$, we must find a consistent basis for their depth. The time average location of the interface between two layers is estimated by the mean of the layers time average depth. Simply put, the density ratio is plotted in-between each pair of layer slope estimates. The alternative, calculating the time average depth of the interface between two layers, is biased by the missing data points in the time series such that the time average interface depth does not occur in-between the time average depth of the layers. Because of this contradiction the layer slope data are plotted at the time average depth of a layer as described above while the density ratio on the interfaces is plotted in-between each pair of layers. The error bars show the variance of the time-mean density ratio derived from equation 3.3 and the estimated error of the linear fit for $\mathcal{R}_L$. Though error bars are shown, no attempt has been made to propagate the errors through the calculations from the observations to results. Nonetheless, I am confident that the observed systematic variation of $\mathcal{R}_L$ with depth, and the associated inverse relationship of $\mathcal{R}_\rho$ and $\mathcal{R}_L$ are significant.

It is tempting to conclude, as in the laboratory experiments of Lambert and Demenkow (1972), that the observed layer slope must be a direct estimate of the buoyancy flux ratio, γ. The estimated flux ratio as a function of density ratio using Stern's formula is plotted on the same lower axis of figure 3-7. While the variation of γ with depth is correlated with the observed $\mathcal{R}_L$, both the magnitude of the flux ratio and the magnitude of its variation with depth are smaller than that of the layer slope. Further consideration must be given to the interpretation of these data and how they are related.

Before continuing with that analysis a few last comments about the observations and the analysis thus far are required. Layers 1, 7, 13 and 14 have been removed in figure 3-7 because they do not fit the trends in the central layers shown. These layers were also removed from the difference time series for the estimate of density ratio shown. The top and bottom of the staircase might be expected to behave differently due to the intermittent layer dynamics. The anomalously low $\mathcal{R}_L = 0.82$ of layer # 7 seems similar in that the layer is not as clearly defined as its neighbors above and below. It appears to be both thinner and more intermittent. Layer # 7 does have an inversely high density ratio when included in the estimates but I feel the explanation is likely to lie in the layer definition used in the temperature-salinity correlation rather than an exception to the staircase physics.

There is a tremendous amount of information contained in the potential temperature salinity scatter plot. It contains 218,304 observations. In the 775 profiles through the layers, the estimated number of observations in each layer is somewhere between 1000 and 6,000, depending on the average layer thickness. The linear fits used to define a layer throw out most of this information to remove the clutter in favor of fitting a line to between 20 and 100 points defined by the maxima of the binned histogram. The resulting slopes are sensitive to the size of
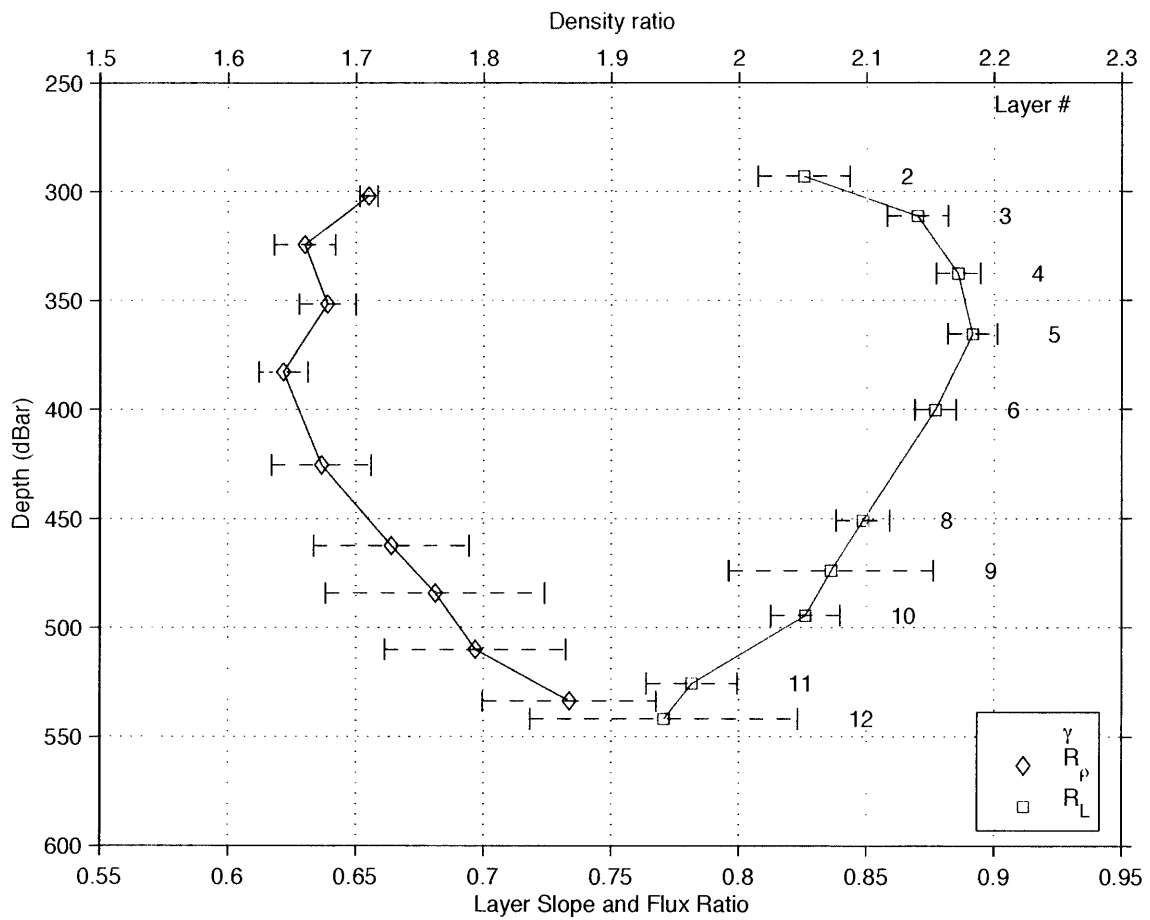
Figure 3-7: Observational results from the moored profiler, including the estimated layer slope, $\mathcal{R}_L$, the mean density ratio, $\mathcal{R}_\rho$, and the estimated flux ratio, γ using Stern's model.

41

the bin used to make the histogram. In identifying 14 layers we determined only 28 values from the entire data set. Future work should involve a more rigorous statistical statement of what defines a layer. Cluster based algorithms (Dasgupta and Raftery, 1998) which are used to find mine fields among background clutter in aerial photographs (Byers and Raftery, 1996) seem like a promising approach to move forward here. Using such techniques would make better use of the available observations in a manner more natural to the data set and would allow a proper estimate of confidence intervals for the results. The statistical techniques could also be applied to a raw form of the data which has ten times the vertical resolution of the two decibar data used here and would achieve ten times the resolution in layer height. This would allow us to examine the dynamics of layer and interface thickness.

The results presented here are an attempt to quantify a visually observable feature of the temperature salinity diagram shown in figure 3-4. The analysis used is the most straight forward route to estimate physical parameters (layer slope and interface density ratio). The significance of the results is self evident in the graphical representation of the data. As long as the interpretation of these results does not over step the limitations set by our assumptions in these calculations our methods are consistent with our analysis. Here we only seek to test whether theory is consistent with the general trends of the observations.

3.5   Extension of Lambert and Demenkow to Oceanic Layers

Recall that in a two layer tank experiment the ratio of the change of temperature to the change of salinity, or the slope of the temperature-salinity diagram, is equal to the flux ratio. Recognizing that two of the assumptions on which this conclusion is based do not hold in the ocean, we consider how to properly extend this conceptual model of $\mathcal{R}_L$ to the ocean. In a tank there is no flux through the boundaries (the sides, top and bottom of the tank) such that the flux across the interface is equal to the flux divergence in a layer. The boundary conditions are more complex in the ocean. Second, in the laboratory the entrainment velocity can be neglected in one layer (experimentally the upper one) since fluid leaving the layer does not change its temperature or salinity. In the ocean staircase this assumption is not valid because each layer is bounded by salt fingers at top and bottom. Thus, the conservation of temperature and salinity takes on a more complicated form in the ocean. If the horizontal velocity in the ith layer is u_i, while the vertical entrainment velocity is $w_{\pm}^{\star}$ at the top or bottom of a layer, then the conservation of volume for a fluid column of constant area whose height changes with the layer may be written $\frac{\partial h_i}{\partial t} + \nabla \cdot (h_i u_i) = w_+^{\star} - w_-^{\star}$. With this statement of conservation of layer thickness, h_i, assuming a linear equation of state we may now write a consistent statement of
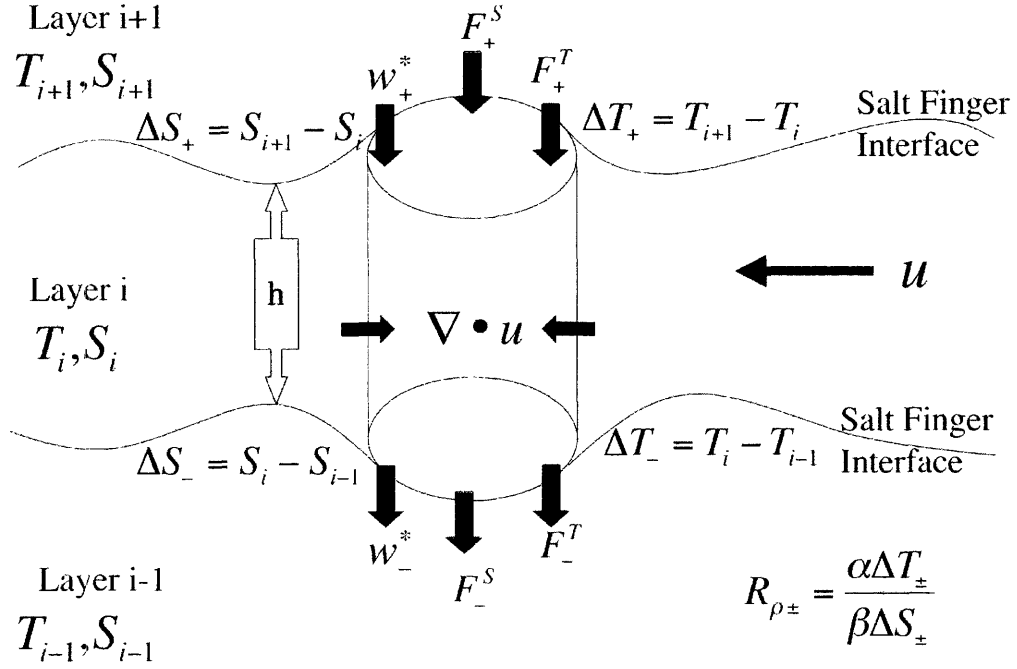
Figure 3-8: Diagram of the terms in equations 3.8 and 3.9.

the conservation of heat, $(h_i T_i)$ and salt, $(h_i S_i)$ integrated over the height of a layer as follows. A diagram of the terms is included in figure 3-8.

$$\frac{\partial(h_i T_i)}{\partial t} + \nabla \cdot \mathbf{u}_i(h_i T_i) = T_{i+1}\mathbf{w}_+^\star - T_{i-1}\mathbf{w}_-^\star + \mathcal{F}_+^T - \mathcal{F}_-^T \tag{3.4}$$

$$\frac{\partial(h_i S_i)}{\partial t} + \nabla \cdot \mathbf{u}_i(h_i S_i) = S_{i+1}\mathbf{w}_+^\star - S_{i-1}\mathbf{w}_-^\star + \mathcal{F}_+^S - \mathcal{F}_-^S \tag{3.5}$$

In deriving these equations, we have made use of the observation that the interfacial velocity is always upward in laboratory experiments and the entrainment velocity, $\mathbf{w}^\star$, will therefore always be negative. Though strongly supported by the laboratory data, the negative entrainment velocity is an assumption which we will further idealize to close the conservation equations. Rearranging terms using the total derivative, $\frac{D(*)}{Dt} = \frac{\partial(*)}{\partial t} + \mathbf{u}_i \cdot \nabla(*)$ the left hand side of equations 3.4 and 3.5 may be rewritten as follows to express conservation of depth-averaged temperature and salinity in a layer.

43

$$h_i \frac{D(T_i)}{Dt} + T_i \overbrace{\left[\frac{\partial h_i}{\partial t} + \nabla \cdot (u_i h_i) \right]}^{\mathcal{H}} = T_{i+1} w_+^\star - T_{i-1} w_-^\star + \mathcal{F}_+^T - \mathcal{F}_-^T \qquad (3.6)$$

$$h_i \frac{D(S_i)}{Dt} + S_i \overbrace{\left[\frac{\partial h_i}{\partial t} + \nabla \cdot (u_i h_i) \right]}^{\mathcal{H}} = S_{i+1} w_+^\star - S_{i-1} w_-^\star + \mathcal{F}_+^S - \mathcal{F}_-^S \qquad (3.7)$$

The term $\mathcal{H}$ in equations 3.6 and 3.7 is the left hand side of the thickness conservation equation which we started with. By making a substitution for $\mathcal{H} = w_+^\star - w_-^\star$ the conservation of layer temperature and salinity may be written neatly (dropping the i subscript) in terms of the difference of temperature and salinity between layers. This derivation is analogous to that for the conservation of potential vorticity in the layers of the wind driven thermocline (Joseph Pedlosky, personal communication).

$$h \frac{DT}{Dt} = w_+^\star \Delta T_+ + \mathcal{F}_+^T - \mathcal{F}_-^T \qquad (3.8)$$

$$h \frac{DS}{Dt} = w_+^\star \Delta S_+ + \mathcal{F}_+^S - \mathcal{F}_-^S \qquad (3.9)$$

Our goal is to explicitly take the ratio of these equations to derive an expression for the flux divergence ratio independent of the layer thickness h in analogy to Lambert and Demenkow (1972) using the layer slope, $\mathcal{R}_L$. We will quantitatively neglect any lateral flux convergence but comment on its impact in the next section.

3.6 Conservation of $\beta S + i\alpha T$: Graphical Solutions

A graphical solution to these equations which can be plotted on the θ–S diagram is intuitive to the way in which the terms act on the temperature and salinity of a layer. Equation 3.8 is multiplied by $\alpha\sqrt{-1}$, and equation 3.9 is multiplied by β. Adding the results and regrouping terms we have:

$$h \overbrace{\frac{D(\beta S + i\alpha T)}{Dt}}^{a} = w_+^\star \overbrace{(\beta \Delta S_+ + i\alpha \Delta T_+)}^{b} + \overbrace{\beta(\mathcal{F}_+^S - \mathcal{F}_-^S) + i\alpha(\mathcal{F}_+^T - \mathcal{F}_-^T)}^{c} \qquad (3.10)$$

The solution requires both the real and imaginary parts of **a**, **b** and **c** sum to zero such that when plotted in $(\beta S, i\alpha T)$ space, the solution is a triangle (Figure 3-9). The slope of the segment corresponding to the term labeled **a** is the time

44

(a) Changes of T, S
    following a layer
(b) Equivalent flux
    divergence by w*
(c) Flux divergence
    due to salt fingers

R_ρ

Isopycnal
Slope

$i\alpha T$

R_L

(c)

(b)

(a)

βS
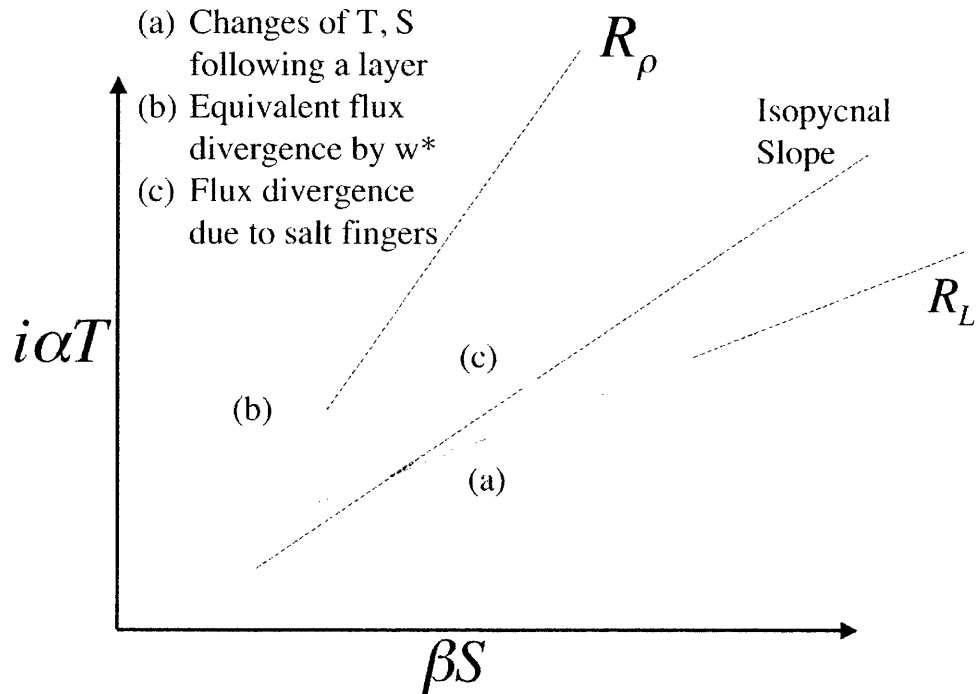
Figure 3-9: Graphical solution to the complex flux divergence equation.

rate of change of the vector $(\beta S, \alpha T)$. We have observed the slope of this vector, $\mathcal{R}_L$ to be constant for each layer over the duration of the moored profiler layer time series. The length of the vector is scaled by the layer thickness. The slope of vector **b** is equal to the density ratio, $\mathcal{R}_\rho$. The length of this vector is scaled by the vertical entrainment velocity **w***. The third vector, labeled **c**, is the salt finger flux divergence of heat and salt across the layer. The implication is that in the thermohaline staircase, the sum of **b** and **c** has a slope equal to $\mathcal{R}_L$ on a range of time scales from days to months. We now see that the variation of this slope over the height of the staircase is related to the density ratio, which appears directly in term **b**, but is also implicated in term **c** from our previous knowledge of salt finger fluxes. In particular, we hypothesize that the inverse correlation of $\mathcal{R}_L$ (decreasing) with $\mathcal{R}_\rho$ (increasing) at the top and bottom of the staircase suggests that changes in the flux ratio with density ratio from one interface to the next are the cause of the flux divergence implied by the variation in layer slope.

This system can be adapted to include isopycnal flux convergences as well. It is interesting to hypothesize about the slope that an isopycnal flux convergence might have in θ—S space. The graphical solution with this addition would be a

quadrilateral. In further discussing the implications of our observations we will assume that the vertical flux convergence terms are an order of magnitude larger than lateral terms, which will be neglected. Based on this physical understanding of the terms involved, we will derive an expression for the scalar slope of the flux divergence ratio as in McDougall (1991).

3.7 A Scalar Equation for the Vertical Flux Divergence Ratio

In the previous section we assumed that the layer slope, defined as $\mathcal{R}_L = \frac{\alpha \partial_t T}{\beta \partial_t S}$ observed by the mooring, is in fact equivalent to $\mathcal{R}_L = (\alpha \frac{DT}{Dt})/(\beta \frac{DS}{Dt})$ in term **a** (Equation 3.10). For this assumption to hold the ratio of both the local temporal and spatial gradients must be constant and equal to the layer slope. This is physically demanded by the observations such that in an arbitrary flow field at an arbitrary mooring location (13°N 55°W) the layer slope $\mathcal{R}_L$ is constant in time for each layer. The spatial survey of the C-SALT experiment described by Schmitt et al. (1987) suggests a uniform layer slope, without vertical variation. While we have observed vertical variations, the C-SALT findings support our statement that a fixed linear relationship of temperature and salinity exists over a broad region of continuous staircase layers. We therefore assert that the layer slope observed by the Moored Profiler (the local time rate of change), is necessarily equal to the ratio of the total derivative of temperature and salinity. Our only assumption is that the mooring location is not unique but rather a representative observation of the constant linear relationship of temperature and salinity for each of the staircase layers. Applying this equivalence to equations 3.8 and 3.9, we write a scalar expression for the flux divergence ratio in terms of the $\mathcal{R}_L$ and $\mathcal{R}_\rho$. These expressions are analogous to the phase of the terms in equation 3.10.

$$\mathcal{R}_L = (\alpha \frac{DT}{Dt})/(\beta \frac{DS}{Dt}) \tag{3.11}$$

$$\alpha h \frac{DT}{Dt} = \mathcal{R}_L h \beta \frac{DS}{Dt} \tag{3.12}$$

$$\alpha(w_+^\star \Delta T_+ + \mathcal{F}_+^T - \mathcal{F}_-^T) = \beta \mathcal{R}_L (w_+^\star \Delta S_+ + \mathcal{F}_+^S - \mathcal{F}_-^S) \tag{3.13}$$

$$w_+^\star (\alpha \Delta T_+ - \beta \mathcal{R}_L \Delta S_+) = \beta \mathcal{R}_L (\mathcal{F}_+^S - \mathcal{F}_-^S) - \alpha(\mathcal{F}_+^T - \mathcal{F}_-^T) \tag{3.14}$$

$$(w_+^\star \beta \Delta S_+)[\mathcal{R}_\rho - \mathcal{R}_L] = \beta(\mathcal{F}_+^S - \mathcal{F}_-^S)[\mathcal{R}_L - \omega] \tag{3.15}$$

$$\mathcal{R}_L - (\frac{w_+^\star \Delta S_+}{\mathcal{F}_+^S - \mathcal{F}_-^S})[\mathcal{R}_\rho - \mathcal{R}_L] = \omega \tag{3.16}$$

$$\omega = \frac{\alpha(\mathcal{F}_+^T - \mathcal{F}_-^T)}{\beta(\mathcal{F}_+^S - \mathcal{F}_-^S)} \tag{3.17}$$

Equation 3.16, derived in McDougall (1991), allows one of the unknowns, **h**, in the unique vector solution for the triangle (Equation 3.10) to be divided out in favor of a ratio of the other two unknowns. The geometric interpretation is that the equation for the flux divergence ratio is analogous to the solution for a similar triangle of fixed proportions but unknown scale. All three angles of a triangle's vertices are determined if one angle and the ratio of the length of two sides are known. The flux divergence ratio, ϖ is the complex phase of term **C**. ϖ can be expressed by the phase of the other two triangle legs, ($\mathcal{R}_L$ and $\mathcal{R}_\rho$) and an unknown ratio of the length of two sides, $(\mathbf{w}_+^\star \Delta S_+)/(\mathcal{F}_+^S - \mathcal{F}_-^S)$. This ratio compares the rate of water mass conversion due to diapycnal advection to that due to salt finger flux convergence. The resulting system of equations is not closed when integrated over the height of the staircase because there are more unknowns than equations. Following McDougall (1991) we continue exploring the constraints that the observations of temperature and salinity in the staircase layers place on the fluxes by relating the buoyancy flux divergence ratio, derived here, to the gradient of the buoyancy flux ratio. The results show that the Stern model for small scale salt finger flux ratio as a function of density ratio is only compatible with the flux divergence ratio of the staircase under very restricted conditions.

Chapter 4

McDougall's Equation for Buoyancy Flux Ratio

Before we begin our analysis, the conclusions of McDougall (1991) should be summarized and the new features of our approach delineated. The CSALT data described a fixed layer slope $\mathcal{R}_L$ which appeared to be constant over the vertical extent of the staircase. McDougall's analysis did "not attempt [ed] to answer the question of why the scaled lateral heat-to-salt ratio is observed to be constant at 0.85. Rather, this constant ratio has been taken as given and the simplest combination of physical processes has been sought to be consistent with it" (McDougall, 1991). In this respect, our analysis is similar to McDougall's. We explore several possible flux balances which satisfy the given observations, however, a mechanistic explanation of the layer slope, the "why," remains out of reach.

McDougall included the same physics for the conservation of depth-averaged temperature and salinity which we have described in the previous chapter. His analysis tested increasingly complex equations for the flux divergence ratio, eventually including the sign and order of magnitude of the lateral flux convergence. McDougall states,

> "It was a surprise to find that the constant value of the lateral heat-to-salt ratio, $\mathcal{R}_L$, together with the requirement of only small vertical variations of the flux ratio, implied rather tight constraints on *both* the flux ratio and the entrainment coefficient rather than simply providing a constraint on some combination of these parameters."

McDougall shows that $\gamma = \mathcal{R}_L$ is the only satisfactory solution but not for the same reasons suggested by the laboratory tank experiments where this is true. By imposing a salt flux maximum at the center of the staircase and attempting to account for the non-linear equation of state, McDougall does indeed place strong constraints on the form of the solution for flux ratio as we shall see. To explain the discrepancy between his model's prediction for the flux ratio and estimates from previous work, McDougall invokes turbulent mixing as a way to boost the salt

finger flux ratio back toward one, while still holding it constant with depth.

We set out to test the effects of the variation of $\mathcal{R}_L$ observed in the staircase by the Moored Profiler. We hypothesized that the inverse correlation of $\mathcal{R}_L$ and $\mathcal{R}_\rho$ might loosen the constraints of McDougall's analysis so that the small scale salt finger physics could be reconciled with the staircase flux divergence without invoking turbulent mixing to raise the flux ratio.

Finally, McDougall summarizes the effect of the entrainment which we sought to describe in the previous chapter.

> "The buoyancy flux ratio of the combination of salt-fingering and entrainment is little different to that of salt-fingering alone. But this small amount of entrainment has a large influence on the evolution of the layer properties because the vertical advection of fluid through the interfaces inherently acts as a *flux divergence* for scalars rather than as a *flux*, and so is much more effective at water-mass conversion than its small effect on the flux ratio would imply. ... It is also very common to confuse fluxes and flux divergences in our thinking. Observed changes in fluid properties in the ocean are always due to flux divergences."

4.1   The Flux Ratio Equation

Our observations of layer temperature-salinity slope and interface density ratio do not yield a unique solution for the flux divergence ratio. However, the observed density ratio profile is sufficient to evaluate the profile of the flux ratio in the staircase if we apply Stern's (1975) model. We proceed by relating the terms which describe the variation of flux ratio with height to the flux divergence ratio. The form of the solution places strong constraints on the shape of the heat and salt fluxes so that an answer, consistent with both our previous models for the flux ratio and our new observations of the layer slope, determines a particular balance of terms. This solution relies on Stern's linear model to provide a boundary condition. We expect this linear model of the salt finger flux ratio to be relevant based on previous laboratory, theoretical and numerical work (St.Laurent and Schmitt, 1999; Schmitt, 1979; Radko, 2003). The comparison of the two models is an effort to show that our understanding of two separate physical scales are consistent and should not be misconstrued as a general solution for staircase dynamics.

On evaluating Stern's model of flux ratio from our observations of the time-mean density ratio across layers, we find that the flux ratio changes slightly with depth (Figure 3-7). From inspection of the terms in the flux ratio (Equation 4.1) we see that this may happen in one of three ways: the heat flux may have a divergence; the salt flux may have a divergence; or finally the ratio of the thermal expansion and haline contraction coefficients may be divergent. This may be written formally by expanding the terms of the derivative of the flux ratio with height.

$$\gamma(z) = \frac{\alpha(z)\mathcal{F}^{\mathsf{T}}(z)}{\beta(z)\mathcal{F}^{S}(z)} \tag{4.1}$$

$$\frac{\gamma_z}{\gamma} = \frac{\mathcal{F}_z^{\mathsf{T}}}{\mathcal{F}^{\mathsf{T}}} - \frac{\mathcal{F}_z^{S}}{\mathcal{F}^{S}} + \frac{(\alpha/\beta)_z}{(\alpha/\beta)} \tag{4.2}$$

The derivatives have been written as subscripts to be compact. It is implicit in this conception that the derivatives exist and are well defined in a continuous sense. Equation 4.2 has units $[\mathrm{m}^{-1}]$ or one over the scale height. The flux ratio scale height is equal to the sum of the scale height of the salt flux, the heat flux and the term due to the nonlinear equation of state, respectively.

$$\frac{1}{H_\gamma} = \frac{1}{H_\mathsf{T}} - \frac{1}{H_S} + \frac{1}{H_{\alpha/\beta}} \tag{4.3}$$

The only one of these terms which can be assessed directly from the data is $H_{\alpha/\beta}$. This scale height describes the effect of the mean temperature and salinity on the equation of state. From the mean profile of temperature and salinity at the Moored Profiler site, we can expect $3 \times 10^3 > H_{\alpha/\beta} > 5 \times 10^2$ (m).

Further rearranging terms in equation 4.2 we can eliminate the unknown heat flux term in favor of the flux divergence ratio, ω, for which we have previously derived an expression (Equation 4.5, McDougall, 1991) .

$$\omega \equiv \frac{\alpha\mathcal{F}_z^{\theta}}{\beta\mathcal{F}_z^{S}} \tag{4.4}$$

$$\gamma_z = -\gamma \left[\frac{\mathcal{F}_z^{S}}{\mathcal{F}^{S}} - \frac{(\alpha/\beta)_z}{(\alpha/\beta)} \right] + \frac{\mathcal{F}_z^{S}}{\mathcal{F}^{S}}\omega \tag{4.5}$$

We now have a first order, linear, ordinary differential equation for the flux ratio with an in-homogeneous term expressed by the flux divergence ratio and the salt flux scale height. A solution to such an equation is guaranteed to exist for arbitrary functional forms of the parameters, which is certainly encouraging. However, the homogeneous term will generally be of an exponential form, $\gamma(z) \sim \exp[z/H_{\gamma(z)}]$. This analysis begins to expose the fundamental conflict between our model of the flux ratio, being exponential, and our observations of density ratio, from which we predict a nearly constant flux ratio. This can only be satisfied by $\lim[H_\gamma \to \infty]$. Without actually solving the ODE we can examine solutions to the equation 4.5 in terms of the scale heights to better understand the terms and their implications. Applying the condition that the flux ratio be constant, $\gamma = \gamma_c$ we have:

$$\lim_{H_\gamma = \infty} \frac{1}{H_\gamma} = -\frac{1}{H_S} + \frac{1}{H_{\alpha/\beta}} + \frac{1}{H_S}\left(\frac{\omega}{\gamma_c}\right) = 0 \tag{4.6}$$

$$\omega = \gamma_c - \gamma_c \frac{H_S}{H_{\alpha/\beta}} \tag{4.7}$$

In the strict limit that that the solution to the differential equation 4.5 has no variation of flux ratio with height (as in McDougall, 1991), equation 4.7 must be satisfied for every $[z]$. Fitting McDougall's model to the data has placed strong constraints on the terms in the solution. With this expression for the flux divergence ratio we can now apply the model of flux divergence ratio which we derived in the previous chapter, $\omega = \mathcal{R}_L - (\frac{w_i^\star \Delta S_i}{\mathcal{F}_i^S - \mathcal{F}^S})[\mathcal{R}_\rho - \mathcal{R}_L]$. Written in a continuous form, the salt flux divergence in the denominator may be replaced by H_S, making the substitution $1/\mathcal{F}_z^S = (1/\mathcal{F}^S)(\mathcal{F}^S/\mathcal{F}_z^S) = H_S(1/\mathcal{F}^S)$. The physical model of ω from the previous chapter is now written in terms of McDougall's flux ratio ODE.

$$\omega = \mathcal{R}_L - H_S\left(\frac{w^\star S_z}{\mathcal{F}^S}\right)[\mathcal{R}_\rho - \mathcal{R}_L] \tag{4.8}$$

$$\omega = \gamma_c - \gamma_c \frac{H_S}{H_{\alpha/\beta}} \tag{4.9}$$

$$\mathcal{R}_L - \gamma_c = H_S\left(\frac{w^\star S_z}{\mathcal{F}^S}\right)[\mathcal{R}_\rho - \mathcal{R}_L] - \gamma_c \frac{H_S}{H_{\alpha/\beta}} \tag{4.10}$$

As previously stated $w^\star$ is assumed to be negative definite based on laboratory observations. To allow further progress we will take the ratio of $w^\star$ to $\mathcal{F}^S$ as an unknown constant in the vertical. The ratio is an expression for the length of the legs of the flux divergence triangle in the previous chapter. The meaning of the term will be discussed further as we explore the relationship of the layer slope and the flux ratio. McDougall also assumed that the ratio was constant over the height of the staircase, based on the results of his laboratory work on the effects of the nonlinear equation of state. In analogy to McDougall we leave this unknown ratio as a free parameter as we seek the most consistent solution for the flux ratio.

Substituting equation 4.8 into equation 4.9 we arrive at the relationship between the layer slope $\mathcal{R}_L$, observed in the θ–S diagram and the constant approximation of the flux ratio. We will examine this equation in three interesting limits of the scale height ratio, $\frac{H_S}{H_{\alpha/\beta}} = \begin{cases} 0 \\ 1 \\ \pm\infty \end{cases}$. These correspond to three different simple balances which are possible in equation 4.3 when γ is constant such that the left hand side of the equation is zero.

4.1.1 $\frac{H_S}{H_{\alpha/\beta}} = 0$

If the equation of state were linear, there would be no change in (α/β) implying $H_{\alpha/\beta} = \infty$, or the first of the three limits where the scale height ratio is equal to 0. For small entrainment velocities, this solution is similar to those of the tank experiments where $\gamma = \mathcal{R}_L$, however the value predicted, (≈ 0.85) is one third larger than that generally observed in lab, $(\gamma \approx 0.6)$. By setting the difference, $\mathcal{R}_L - \gamma$, equal to the vertical entrainment term, we can estimate the order of magnitude to see if it is physically reasonable.

$$\underbrace{\frac{\overbrace{\mathcal{R}_L - \gamma_c}^{\approx .25}}{\mathcal{R}_\rho - \mathcal{R}_L}}_{\approx .75} = H_S\left(\frac{w^\star S_z}{\mathcal{F}^S}\right) \tag{4.11}$$

We can simplify the form of this equation by assuming a constant eddy diffusivity for salt such that $\mathcal{F}^S = -K_S S_z$. Our assumptions lead to $H_S\left(\frac{w^\star}{K_S}\right) \approx -.3$. This is consistent with our physical intuition that the entrainment velocity should be negative, and the eddy diffusivity of salt, K_S should be positive. Rather than using the nonlinear equation of state and empirical expressions as in McDougall (1991), $w^\star/K_S$ is a somewhat simpler physical interpretation of the entrainment velocity and its importance relative to salt fingering. Under the assumptions in equation 4.11, the scale height H_S must then be positive definite (fluxes are largest at the top of the staircase). Using the Schmitt et al. (2005) estimate of $K_S = 0.9 \times 10^{-4}(m^2 s^{-1})$ in SFTRE and an entrainment velocity of a meter per year we predict a salt flux scale height of roughly 100 (m). Since both the flux ratio and the nonlinear terms have been taken as constant, equation 4.3 implies that $H_S = H_T$. The heat and salt flux have the same functional form and their ratio is constant equal to $\mathcal{F}^T = \mathcal{F}^S(\gamma \frac{\beta}{\alpha})$. Recalling the triangle which the conservation equations satisfy in the previous chapter, the slope of term c (Equation 3.10), equal to the flux divergence ratio, must now have a slope of $\gamma \approx 0.6$ under this set of assumptions.

However, due to the 8°C change in potential temperature between the top and bottom of the staircase the nonlinear term does change significantly. We have estimated $H_{\alpha/\beta} \approx 1000$ (m). The limit we have explored here therefore only applies where $H_S \ll H_{\alpha/\beta} \approx 1000$ (m), a prediction that the heat and salt flux would have to be strongly convergent.

4.1.2 $\frac{H_S}{H_{\alpha/\beta}} = 1$

This second case implies $H_{\alpha/\beta} = H_S$. In this limit we find

$$\mathcal{R}_L = H_S\left(\frac{w^\star S_z}{\mathcal{F}^S}\right)[\mathcal{R}_\rho - \mathcal{R}_L] \tag{4.12}$$

The layer slope is now independent of the flux ratio which has cancelled out of the equation. The order of magnitude estimates used in the previous case (for $\mathbf{w^\star}$ and $\mathbf{K_S}$) can be applied here as well. The result is a scale height roughly three times larger than in the previous case. This limit, $\mathbf{H_{\alpha/\beta}} = \mathbf{H_S}$, also places strong constraints on the heat flux in equation 4.3. Since the flux ratio is constant, the heat flux must now also be constant and the flux divergence ratio, $\omega = 0$. Applying this limit to the conservation equations satisfied in chapter three, the flux divergence of salt is finite, but the ratio plotted in the temperature salinity diagram must have zero slope.

4.1.3 $\quad \dfrac{\mathbf{H_S}}{\mathbf{H_{\alpha/\beta}}} = \pm\infty$

Finally, for very large values of the scale height ratio, (we understand this case by holding $\mathbf{H_{\alpha/\beta}}$ finite, and let $\mathbf{H_S} = \pm\infty$), the only solution possible requires that the left hand side and right hand side of the equation 4.10 balance separately such that when,

$$\mathbf{H_S} = \pm\infty$$

$$\overbrace{\mathcal{R}_L - \gamma_c}^{\dagger} = \mathbf{H_S} \overbrace{\left[\frac{\mathbf{w^\star S}_z}{\mathcal{F}^S}[\mathcal{R}_\rho - \mathcal{R}_L] - \frac{\gamma_c}{\mathbf{H_{\alpha/\beta}}} \right]}^{\ddagger} = 0 \qquad (4.13)$$

Equation 4.13 requires both terms, † and ‡ equal zero independently. The sign and magnitude of terms in ‡ are consistent with what we have already found under other conditions. That result is not physically problematic. However the requirement for † is not physical. The condition for † = 0 sets the flux ratio equal to the layer slope as in McDougall, while salt finger theory and laboratory experiments suggest they are different by ≈ 0.25. Just as McDougall found, no consideration of other physical terms and processes (lateral flux convergence) will remedy this confounding property of the ODE. The general scale height equation (4.3) given this limit for constant flux ratio and constant salt flux, requires that $\mathbf{H_{\alpha/\beta}} = \mathbf{H_T}$. In this case the flux divergence leg of the conservation triangle must be vertical, with zero salt flux divergence. This condition is a consequence of any hypothetical salt flux maximum in the staircase (assuming the flux must be differentiable).

4.2   A Tale of Two Flux Models

Based on physical intuition, McDougall (1991) suggested that the center of the staircase must be a maximum of the downward salt finger flux, which decreases to zero at the top and bottom of the staircase. Using his Gaussian salt flux profile

model we derive H_S,

$$\mathcal{F}^S \equiv \exp[\frac{-(z - z_0)^2}{H_S^2(0)}] \tag{4.14}$$

$$\frac{\mathcal{F}_z^S}{\mathcal{F}^S} = -\frac{2[z - z_0]}{H_S^2(0)} \tag{4.15}$$

$$H_S = -\frac{H_S^2(0)}{2[z - z_0]} \tag{4.16}$$

The salt flux scale height, H_S changes sign at the center of the staircase, $z = z_0$, from positive infinity to negative infinity, with a scale set by the $H_S^2(0) \approx 100^2$. The physically intuitive salt finger flux profile leads to a physically ill-behaved solution. Returning to the scale height equation for constant flux ratio 4.10, in this parameterization of the salt flux profile the staircase must satisfy all three limits we have explored for the scale height ratio, $\frac{H_S}{H_{\alpha/\beta}} = \begin{cases} 0 \\ 1 \\ \pm\infty \end{cases}$. McDougall found the only solution possible for constant flux ratio under these conditions requires the flux ratio is equal to the layer slope. As our intuition suggested, allowing for the small variation with height which we observe in $\mathcal{R}_L$ and in the estimated flux ratio would act in the correct sense to push the solution toward the magnitude of Sterns model for flux ratio, but it does not repair the inconsistency caused by the gaussian salt flux profile. If the correct model for flux ratio were steeper than Stern near $\mathcal{R}_\rho = 1.6$, allowing a stronger variation of flux ratio with density ratio, a salt flux maximum might have a tenable physical interpretation. This possibility should be investigated further.

The difficulty lies not in the physics of the layer slopes, but in the shape of the salt flux profile. Lateral flux convergence will not fix this. Only by invoking vertical turbulent mixing could McDougall explain the elevated flux ratio predicted by his model. Given this inconsistent solution, we propose an alternative salt flux profile model. The mean salinity profile is nearly exponential (increasing upward) throughout the staircase. Assumption of a constant eddy diffusivity for salt leads to a simple, constant salt flux scale height. The exponential scale height of the salinity profile sets the salt flux scale height.

$$S = \exp[z/H_\mu] \tag{4.17}$$

$$S_z = \frac{1}{H_\mu}\exp[z/H_\mu] \tag{4.18}$$

$$\mathcal{F}^S = -\kappa\frac{1}{H_\mu}\exp[z/H_\mu] \tag{4.19}$$

$$\mathcal{F}_z^S = -\kappa\frac{1}{(H_\mu)^2}\exp[z/H_\mu] \tag{4.20}$$

$$\frac{\mathcal{F}_z^S}{\mathcal{F}^S} = \frac{1}{H_\mu} \tag{4.21}$$

$$H_\mu = H_S \tag{4.22}$$

The observed salt flux scale height using this method is very nearly equal to that measured for the nonlinear term by a similar exponential fit to the variation of (α/β). This suggests that the salt finger staircase is nearly in the balance described by the second limit (Subsection 4.1.2) for the solution of equation 4.10. The magnitude of the flux ratio is independent of the layer slope since γ cancels out of equation 4.12. As discussed previously the condition for constant flux ratio sets the flux divergence ratio to zero, requiring that the heat flux be constant.

4.3 Solutions to the Differential Equation

We may formally solve the differential equation describing the flux ratio using both models of the salt flux which we have described and examine the solutions in graphical form. Figure 4-1 is similar to that in McDougall (1991) showing flux ratio (the X-axis) as a function of height (the Y-axis) about z_0, the center of the staircase. Solutions are plotted using a constant value of the density ratio and layer slope (blue lines), as well as quadratic fits to the $\mathcal{R}_\rho$ and $\mathcal{R}_L$ observations (red dashed lines). There seems to be little qualitative difference between these solutions. Each axis shows solutions for a different constant value of the entrainment velocity on the eddy diffusivity for salt, $\frac{w^*}{\kappa_S}$. Within each axis a family of solutions to the ODE are plotted with five different values of the boundary condition which must be specified for a unique solution. In McDougall's model the magnitude of the solution at the boundary directly determines its slope at the boundary. The solution which is nearly constant, occurs in the graph for which the coefficient $\frac{w^*}{\kappa_S}$ satisfies equation 4.13 such that $\ddagger = 0$. The unique solution of this family for constant flux ratio is set by $\gamma = \mathcal{R}_L$, such that $\dagger = 0$, as expected from the scale height analysis. The arbitrary boundary condition does not provide the means to let the model flux ratio conform to the value predicted by Stern because the shape of the solution is expressly dependent on the magnitude of the flux ratio. Only in the 2nd limit where the salt flux scale height and the nonlinear scale height cancel, is the
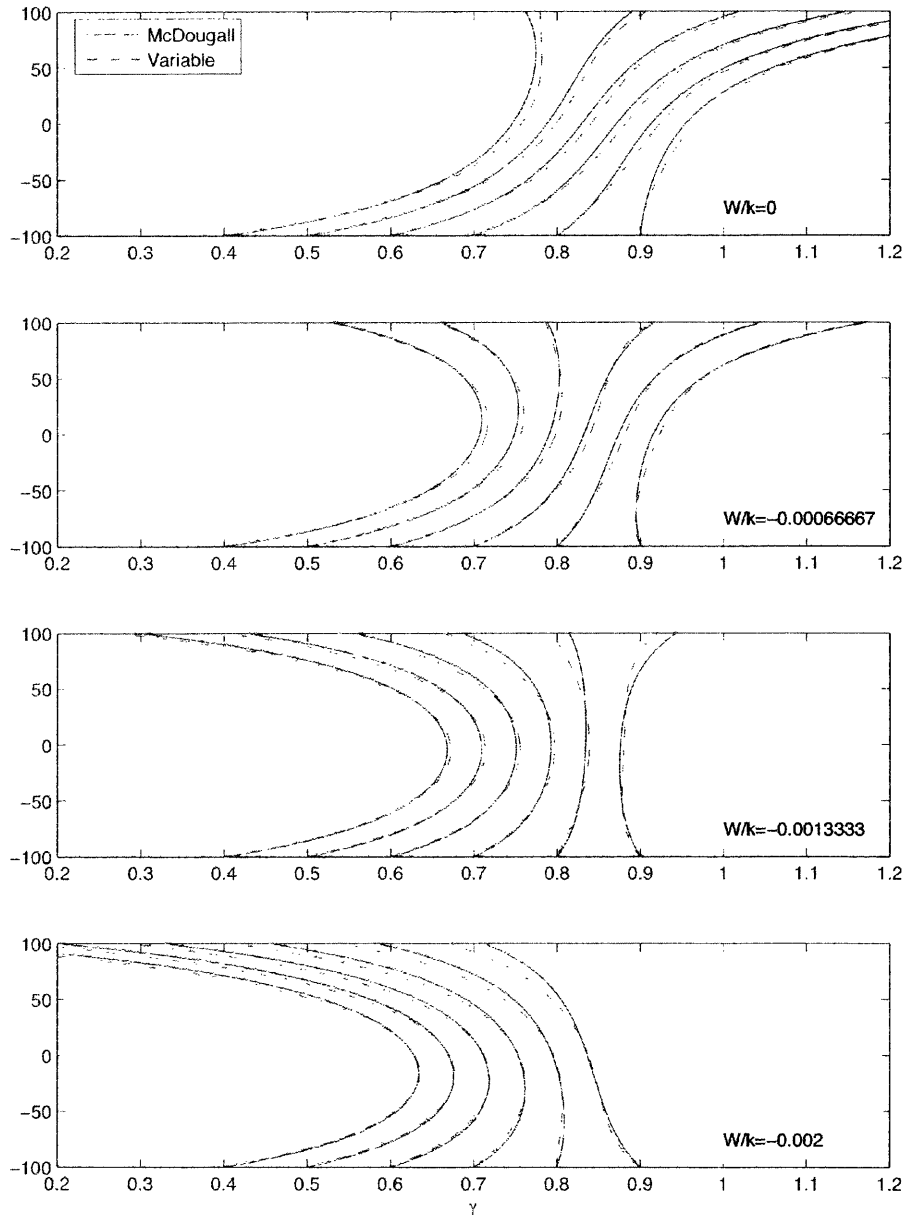
Figure 4-1: Solutions to the differential equation for flux ratio (the x-axis), vs height (the y-axis), using McDougall's gaussian salt flux profile. Each graph represents a different set of solutions for different proportions of the flux divergence triangle set by w/k_s. Each assumption about the relative magnitude of the divergence due to vertical advection vs the salt finger flux divergence yields a particular differential equation. The family of solutions for various boundary condition $\gamma|_{(z=-100)}$ is plotted in each graph. The solid blue curves are McDougall's solution from 1991. The red dashed curves include a quadratic fit to the observed variation of $\mathcal{R}_\rho$ and $\mathcal{R}_L$ in the SFTRE data. The character of the solutions is dominated by the salt flux model. Including the observed variation with height of the flux divergence terms makes little difference in the solutions for the flux ratio.

magnitude of the solution independent of its gradient.

The exponential model for the salt flux which we proposed, based on the shape of the salinity profile, allows the magnitude of the solution to be arbitrary as in the second limit (Subsection 4.1.2). From the observations we find that the α/β profile and the salinity profile have nearly the same scale height. The difference in scale heights is estimated to be, $H_S - H_{\alpha/\beta} \approx 10^2$, roughly ten times smaller than the magnitude of either term individually. Due to the very small difference between these terms the shape of the flux ratio profile is nearly independent of the magnitude set at the boundary (Figure 4-2). The family of curves in each graph are all possible solutions. The ODE alone can not discriminate between them. The different axes are solutions using different estimates of the entrainment velocity, similar to the solutions in the previous figure. The solution which is most nearly constant occurs when the entrainment velocity is such that the heat flux through the staircase is constant. The red dashed lines are the full solution using the scale height estimated from observations. The black line is the limit in which the scale heights are equal but $\mathcal{R}_\rho$ and $\mathcal{R}_L$ are set by the observations, while the blue curves are integrated with $H_S - H_{\alpha/\beta} = 0$ and $\mathcal{R}_\rho$ and $\mathcal{R}_L$ constant and equal to 1.6 and 0.85, respectively. This solution is physically different from McDougall's. The magnitude of the flux ratio is not determined by the ODE because the homogenous term of the solution is small. The exponential salt flux allows us to match the magnitude estimated by Stern's formula. The quadratic fit to the variation of layer slope and density ratio cause the solution for the flux ratio to be cubic. The ODE predicts γ should have a maximum and minimum or an inflection point. This does not fit the character of our flux ratio estimates from Stern's density ratio model. Still, if the mechanism by which the equation has allowed us to set the magnitude of the flux ratio (if not its structure) is physical, it suggests there must be a link between the salt flux scale height and the non-linear equation of state such that these terms balance as the system evolves.

The solutions which we have compared graphically can be derived from the general solution to first order linear ordinary differential equations. Consider the form of the solution for Y using the integrating factor method for arbitrary functions, f and g:

$$d_t Y(t) + f(t)Y(t) = g(t) \tag{4.23}$$

$$\text{let} \quad \mu(t) \equiv \exp[\int^t f(t')dt'] \tag{4.24}$$

$$d_t(\mu(t)Y) = \mu(t)g(t) \tag{4.25}$$

$$Y(t) = \frac{\int^t \mu(t')g(t')dt' + C}{\mu(t)} \tag{4.26}$$

The solutions calculated by McDougall using the Gaussian salt flux, $(f \sim z)$ have the general form $\gamma \sim \text{erf}(z) + C \exp(z^2)$. The arbitrary constant C, specified by the
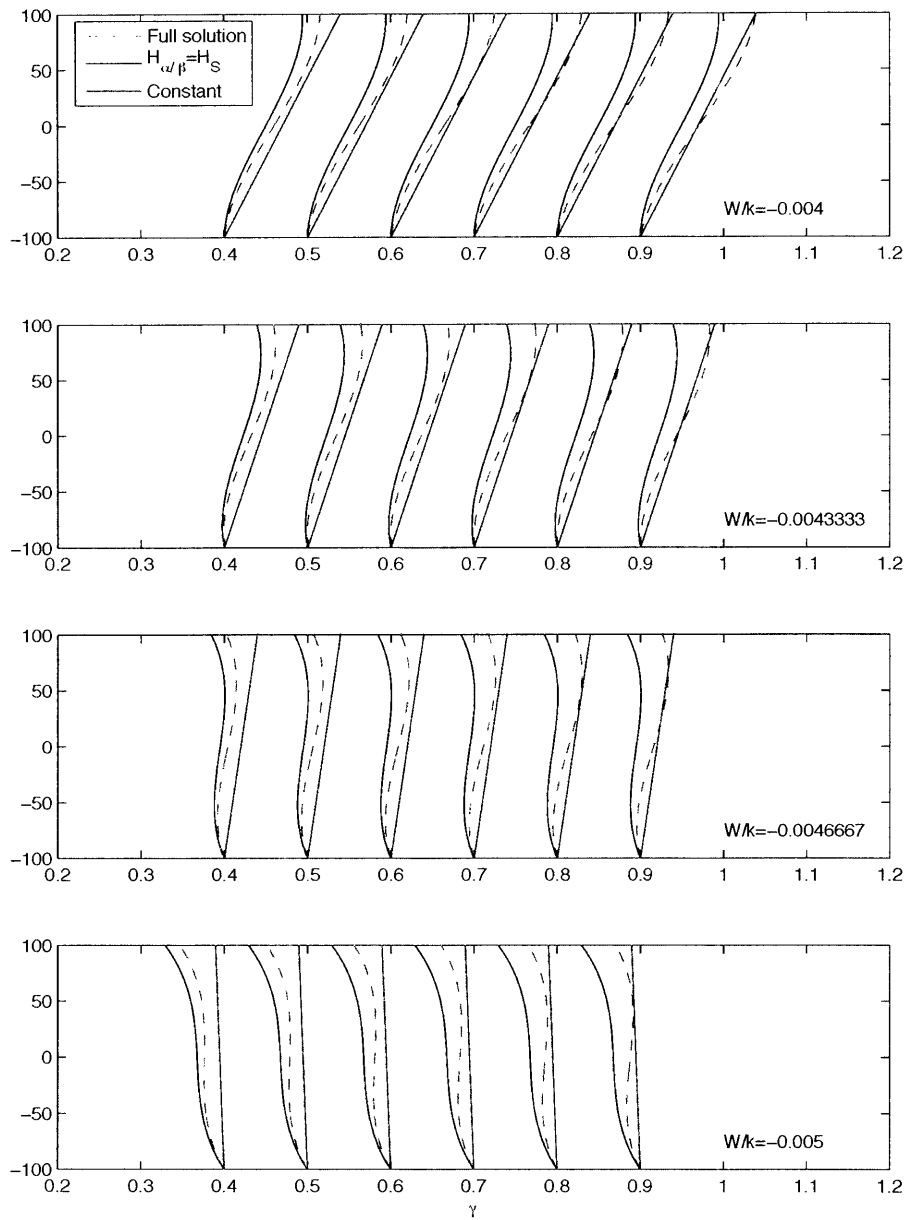
Figure 4-2: Similar to the previous figure, these are the solutions to the differential equation for the flux ratio vs height using the exponential model of the salt flux. The red dashed curve is the full solution using the same quadratic estimate of $\mathcal{R}_\rho$ and $\mathcal{R}_L$. The other two curves (blue and black) are solutions in the limit that the salt flux scale height is equal to the nonlinear scale height. In the blue curves the variation of $\mathcal{R}_\rho$ and $\mathcal{R}_L$ has been neglected similar to McDougall's solution.

boundary condition, is free to set the value of γ at only one location, while determining the shape of the solution for all z. Analogous to the scale height discussion, only when $\frac{g(t)}{f(t)}$ is constant can there be a constant solution to the differential equation. In the limit that $f(t) = 0$ for all t, or in the flux ratio problem, when the scale heights (H_S, $H_{\alpha/\beta}$) are equal, the solution becomes the integral of one over the heat flux scale height. The solution is constant when the heat flux scale height is infinite or the heat flux is constant. The solutions plotted in figure 4-2 are degenerate solutions to the differential equation for flux ratio. The ODE is reduced to, $\gamma_z = 0$ when the solution is constant with height.

4.4 Discussion

The temperature salinity time-series from the SFTRE Moored Profiler provides a new basis to study the implications of the empirically time-invariant slope $\mathcal{R}_L$ (potential temperature-salinity space), of the staircase layer water properties. The analysis of the C-SALT data by McDougall (1991) provides a context for our study. McDougall concluded that the constant density ratio and constant $\mathcal{R}_L$ observed in C-SALT requires a constant flux ratio in the staircase that is rather higher than normally assumed. Our new observations of the variability of these parameters over the height of the staircase lead us to incorporate certain aspects of salt finger physics into the analysis.

Following McDougall's treatment we construct a ratio of terms from the passive tracer evolution equations for heat and salt which describe the observed relationship of temperature and salinity. This places a strong but non-unique constraint on the vertical flux divergence of heat and salt in these equations. Ignoring lateral flux convergence, we arrive at the three-term solution presented in chapter three. Physically these equations state that both temporal gradients and horizontal spatial gradients of water mass properties in a layer must occur in a fixed ratio given the observed relationships. With the assumption that vertical processes dominate the flux convergence, thereby setting $\mathcal{R}_L$, the decomposition of the conservation equations leaves two terms. These consist of an advective transport of water by the mean vertical velocity between the layers (which inherently acts as a flux divergence for layer properties), and a direct flux divergence term. Here, flux refers to the turbulent correlation of the residual vertical velocity with temperature and salinity in the salt fingers. The flux divergence represents the difference between the salt finger fluxes at the top and at the bottom of a layer. The vector sum of these components in temperature-salinity space is the time rate of change of layer water mass properties.

Given this physical interpretation of the large scale processes we apply Stern's salt finger theory governing the small scale fluxes, seeking a single consistent solution. The new estimates of mean density ratio in the staircase suggest that the vertical flux due to salt fingers (ignoring possible lateral flux divergence terms)

is the dominant process in the staircase. This is the basis of our assumptions in the previous paragraph. To evaluate the contribution of the turbulent flux due to the small-scale salt fingers to the large-scale staircase we refer to analytic salt finger theory. From the variety of evidence suggesting that the flux ratio depends strongly on the density ratio, we have chosen to apply Stern's (1975) model which is the simplest model to capture the relevant aspect of the physics which we wish to test. The analysis places limits on our conclusions. We can show that given our observations of temperature and salinity, Stern's salt finger flux ratio model of density ratio dependence is consistent (or not) with the constraints on the flux ratio implicit in the conservation equations.

These two models, one for the large scale flux divergence of the staircase and the other for small scale fluxes of the salt fingers are related by an ordinary differential equation which describes the variation of flux ratio with height. Following McDougall's work we adjust the parameters of the model using an assumption about the salt flux profile to find a solution which is consistent with the salt finger staircase physics we have incorporated. In examining the Gaussian salt flux profile proposed by McDougall we conclude as he did that the solution cannot satisfy both the magnitude and vertical variation of flux ratio which are described by salt finger theory. McDougall's solution required the flux ratio to be greater than that predicted by Stern by one third (0.8 rather then 0.6). The solution to the ordinary differential equation is composed of Error Functions and Gaussians, while our physically motivated analytic theory for salt fingers suggest only a modest flux ratio variation even under our new observations of density ratio (Figure 3.7). The solution that McDougall found to rectify this discrepancy requires three different physical balances between the terms over the height of the staircase (Sections 4.1.1-4.1.3). The Gaussian flux profile requires that the salt flux approach zero at top and bottom while also becoming non-divergent at the center of the staircase. Although a constant flux ratio solution does exist there is nothing to suggest the physics of salt fingers should change from one layer to the next to realize the required flux balances. However, many of these issues would be resolved if the flux ratio had a much stronger dependence on density ratio. If the sensitivity of the flux ratio-density ratio relationship were under estimated in Stern's theory, such that the flux ratio did indeed have a maximum near $\gamma \sim \mathcal{R}_L \sim 0.8$, McDougall's salt flux profile might be consistent.

Following the same approach as McDougall we hypothesize an alternative salt flux profile that rectifies the major discrepancy, the magnitude of the flux ratio, between Stern's model and McDougall's solution. The nearly exponential salinity profile provides the motivation to test a diffusive or exponential salt flux profile in place of McDougall's Gaussian. The resulting change in the nature of the solution to the ODE permits nearly constant solutions for flux ratio with an arbitrary magnitude due to the cancelation of $H_{\alpha/\beta}$ and H_S. Physically the solution compensates the exponential variation of the salt flux with an inverse variation of the
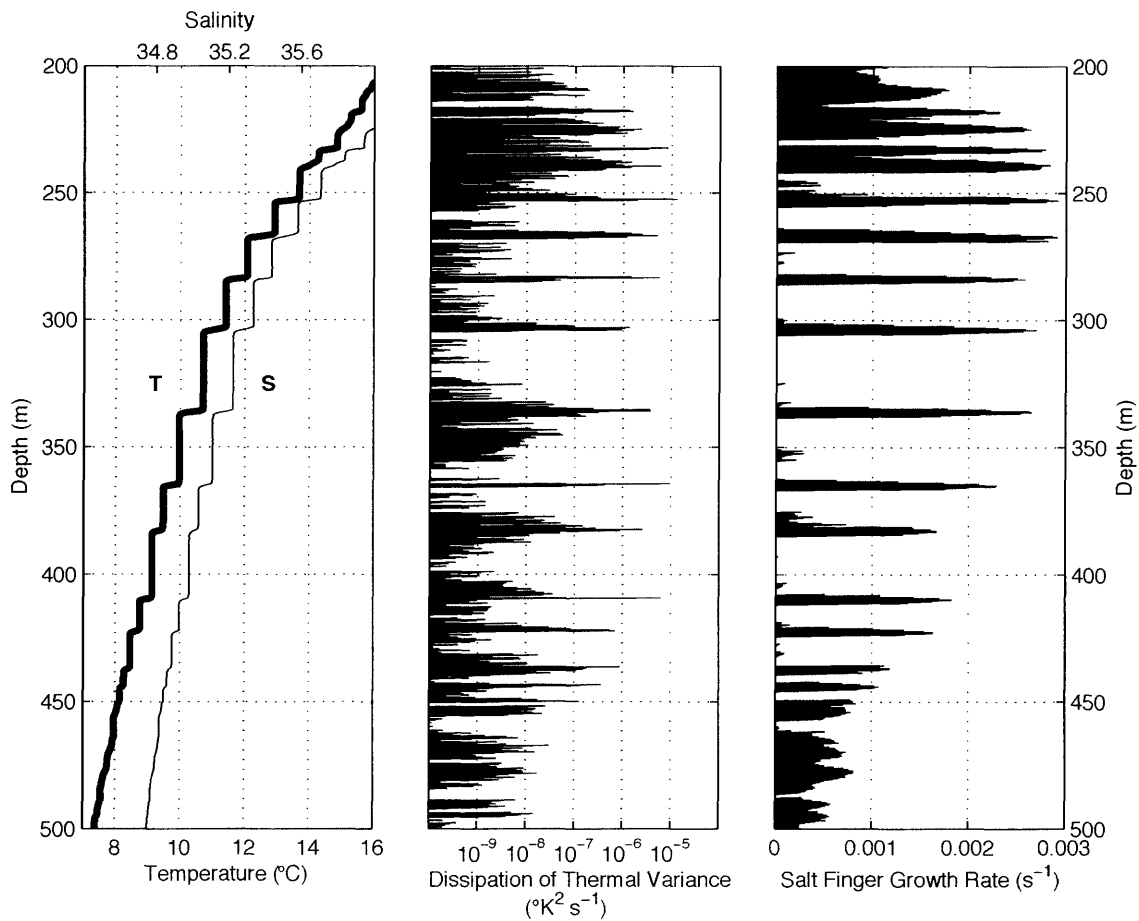
Figure 4-3: Data from the HRP measurements of the salt finger staircase in SFTRE. Note the relatively constant maximum value of the dissipation of thermal variance in each interface. Published by Schmitt etal in Science 2005.

thermal expansion coefficient to maintain a constant flux ratio. This allows the magnitude of the flux ratio to be set by the integration constant satisfying Stern's model. Thus, solutions with a flux ratio near 0.6 and a modest variation in the vertical can be obtained. The physical balance of this consistent solution is of interest because it suggests that the vertical heat flux is nearly constant throughout the staircase. Both the physical dynamics which might explain such a balance and a diagnosis of the predicted heat flux should be investigated further. The HRP data from SFTRE present an opportunity to do so, examining the dissipation of thermal variance in the salt finger interfaces. From this we may estimate the heat flux under the assumption of a dissipation production balance. We note that the values of dissipation maximum which occurs in salt finger interfaces (Figure 4-3) are nearly constant throughout the staircase.

While the exponential salt flux model resolves our concerns about the magnitude of the flux ratio, a further complication lies in the shape of the solution when the model includes a variable density ratio and layer slope. Using the parame-

terizations we tested, the solution now has a maximum and minimum flux ratio within the staircase while the observed density ratio profile suggests (via Sterns model) that there is only one flux ratio maximum. Solving the ODE, the integration of the second order polynomial parameterization of the density ratio yields a third order solution, thus giving an incongruous trend in flux ratio at the bottom of the staircase. In spite of this discrepancy we find the magnitude of the flux ratio determined by the water mass layer slopes is consistent with salt fingering.

In further advancing our understanding of the staircase fluxes, the Stern model could be modified to account for the stronger dependence on density ratio suggested by the observational work of St.Laurent and Schmitt, (1999). This might permit solutions which reconcile the differences between the large-scale water mass conversion model and the small scale salt finger flux model. It may also prove useful to incorporate a density ratio dependent salt flux, such as that proposed by Schmitt (1981), to develop a salt flux convergence profile that responds to the variations in $\mathcal{R}_\rho$.

Finally, another approach for further investigation might lie in rephrasing the question to better handle the mathematical difficulties we have outlined. Through an algebraic manipulation of terms in McDougalls differential equation we can apply Sterns model to solve for the salt flux rather than the flux ratio. Since the salt flux profile would then be arbitrary this changes the number of degrees of freedom of the solution permitting a result for any observed layer slope, density ratio and flux ratio dependence. The vertical advection term would then remain unknown. While this approach would resolve many of the issues we examined concerning the scale height of the salt flux, it is not a solution to McDougall's question, finding a consistent salt flux.

4.5 Conclusion

The SFTRE Moored Profiler time series from the western tropical North Atlantic provides the first continuous time series of temperature, salinity and velocity in a thermohaline staircase. The evolution of layer properties are well documented during the 4.3 month record. Such staircases are associated with strong salt fingering at the interfaces between the mixed layers. These data provide unique insights into the dynamics of the salt finger flux convergence which sets the layer properties. The striking linear correlation between the temperature and salinity of the layers observed in C-SALT is refined by these observations. Instead of the constant $\mathcal{R}_L$ and $\mathcal{R}_\rho$ observed in C-SALT, an inverse relation between the two is observed in vertical profiles. This inverse relationship is suggestive of a physical link between the two.

Revisiting the work of McDougall (1991), we set out to test the implications of the observed vertical variation of the layer slope, noting that the assumption of constant layer slope, constant flux ratio and gaussian salt flux profile may have

63

been too restrictive. In reconstructing McDougall's work using our new observations, the analysis has shown that the result is sensitive to our assumptions due to the form of the ordinary differential equation. McDougall's Gaussian salt flux profile prescribes the flux ratio equal to the layer slope, which is larger than that observed in the laboratory. This condition is not necessitated by the observations but rather by the assumption of the salt flux profile. We have demonstrated that physically motivated solutions do exist in which the ODE is silent about the magnitude of the flux ratio, only setting its vertical structure by the observed variation of layer slope and density ratio. The new model permits a solution for flux ratio which is found to be consistent with the magnitude predicted by Stern's formula and laboratory observations though details of the vertical variation do not fully agree. The physical consequences of the mathematics of our analysis should be investigated further. In particular, the heat flux, which is predicted to be nearly constant through the staircase in our model might be tested with data from the HRP. The consistent solution is contingent upon the cancelation of variation in the salt flux with variation in the thermal expansion coefficient to yield the estimated magnitude of the buoyancy flux ratio. Considerable thought should be given to the mechanism by which this balance is maintained.

Bibliography

[1] S. Byers and A. E. Raftery. Nearest neighbor clutter removal for estimating features in spatial point processes. Technical Report 305, University of Washington, Department of Statistics, University of Washington, Seattle, WA, April 1996.

[2] A. Dasgupta and A. E. Raftery. Detecting features in spatial point processes with clutter via model-based clustering. *Journal of the American Statistical Association*, 93(441):294, 1998.

[3] K. W. Doherty, D. E. Frye, S. P. Liberatore, and J. M. Toole. A moored profiling instrument. *Journal of Atmospheric and Oceanic Technology*, 16:1816–1829, 1999.

[4] E. Kunze. A review of oceanic salt-finger theory. *Progress in Oceanography*, 56:399–417, 2003.

[5] R. B. Lambert and J. W. Demenkow. On the vertical transport due to fingers in double diffusive convection. *Journal of fluid mechanics*, 54:627–640, 1972.

[6] B. Magnell. *Oceanic microstructure near Bermuda using a towed sensor*. PhD dissertation, WHOI/MIT Joint Program, Woods Hole, MA, 1973.

[7] G. O. Marmorino, W. K. Brown, and W. D. Morris. Two-dimensional temperature structure in the C-SALT thermohaline staircase. *Deep-Sea Research*, 23(10):1339–1347, 1987.

[8] T. J. McDougall. Double-diffusive convection with a nonlinear equation of state. part i: Laboratory experiments and their interpretation. *Progress in Oceanography*, 10:91–121, 1981.

[9] T. J. McDougall. Double-diffusive convection with a nonlinear equation of state. part ii: The accurate conservation of properties in a two-layer system. *Progress in Oceanography*, 10:71–89, 1981.

[10] T. J. McDougall. Double-diffusive interleaving. part 1: Linear stability analysis. *Journal of Physical Oceanography*, 15:1532–1541, 1985.

[11] T. J. McDougall. Neutral surfaces. *Journal of Physical Oceanography*, 17:1950–1964, 1987.

65

[12] T. J. McDougall. Interfacial advection in the thermohaline staircase east of Barbados. *Deep-Sea Research*, 38(3):357–370, 1991.

[13] Alexander M. Mood, Franklin A. Graybill, and Duane C. Boes. *Introduction to the Theory of Statistics*, section 2.3, pages 180–181. McGraw-Hill, New York, third edition, 1913.

[14] Joseph Pedlosky. *Ocean Circulation Theory*, section 3.2. Springer-Verlag, Berlin, second edition, 1998.

[15] T. Radko. A mechanism for layer formation in a double-diffusive fluid. *Journal of Fluid Mechanics*, 497:365–380, 2003.

[16] B. Ruddick. Laboratory studies of interleaving. *Progress in Oceanography*, 56:529–547, 2003.

[17] B. Ruddick and A. E. Gargett. Oceanic double-infusion: introduction. *Progress in Oceanography*, 56:383–393, 2003.

[18] B. Ruddick and O. Kerr. Oceanic thermohaline intrusions: theory. *Progress in Oceanography*, 56:483–497, 2003.

[19] B. Ruddick and K. Richards. Oceanic thermohaline intrusions: observations. *Progress in Oceanography*, 56:499–527, 2003.

[20] R. W. Schmitt. The growth rate of super-critical salt fingers. *Deep-Sea Research*, 26:23–40, 1979.

[21] R. W. Schmitt. Form of the tmperature-salinity relationship in the central water: Evidence for double-diffusive mixing. *Journal of Physical Oceanography*, 11(7):1015–1026, 1981.

[22] R. W. Schmitt. On the density ratio balance in the central water. *Journal of Physical Oceanography*, 20(6):900–906, 1990.

[23] R. W. Schmitt. Observational and laboratory insights into salt finger convection. *Progress in Oceanography*, 56:419–433, 2003.

[24] R. W. Schmitt, J. R. Ledwell, E. T. Montgomery, K. L. Polzin, and J. M. Toole. Enhanced diapycal mixing by salt fingers in the thermocline of the tropical Atlantic. *Science*, 308:685–688, 2005.

[25] R. W. Schmitt, H. Perkins, J. D. Boyd, and M. C. Stalcup. An investigation of the thermohaline staircase in the western tropical North Atlantic. *Deep-Sea Research*, 34(10):1655–1665, 1987.

[26] W. J. Schmitz, J. R. Luyten, and R. W. Schmitt. On the Florida current T/S envelope. *Bulletin Of Marine Science*, 53(3):1048–1065, 1993.

[27] Melvin E. Stern. *Ocean Circulation Physics*, section 11.2, pages 191–196. Academic Press, INC., New York, 1975.

[28] L. St.Laurent and R. W. Schmitt. The contribution of salt fingers to vertical mixing in the north atlantic tracer release experiment. *Journal of Physical Oceanography*, 29(7):1404–1424, 1999.

[29] John M. Toole, K. W. Doherty, D. E. Frye, and S. P. Liberatore. Velocity measurement from a moored profiling instrument. In *Proceedings of the IEEE Sixth Working Conference on Current Measurement*, pages 133–139, Woods Hole, 1999. Woods Hole Oceanographic Institution.

[30] A. J. Williams. Salt fingers observed in the mediterranean outflow. *Science*, 185:941–943, 1974.

[31] Carl Wunsch. *The Ocean Circulation Inverse Problem*, chapter 3. Cambridge University Press, Cambridge, 1996.

[32] J. Yoshida and H. Nagashima. Numerical experiments on salt-finger convection. *Progress in Oceanography*, 56:435–459, 2003.

[33] J. Zhang and R. W. Schmitt. The impact of salt fingering on the thermohaline circulation under mixed boundary conditions. *Journal of Physical Oceanography*, 30(6):1223–1231, 2000.